Preliminary development of a novel catamaran floating offshore wind turbine platform and assessment of dynamic behaviours for intermediate water depth application

Joshua Cutler [a], Musa Bashir[a*], Yang Yang[b], Jin Wang[a], Sean Loughney[a]

[a]*School of Engineering, Liverpool John Moores University, Liverpool, L3 3AF, UK*

[b]*Faculty of Maritime and Transportation, Ningbo University, Ningbo, 315211, P.R. China*

Abstract:

This paper presents the preliminary development of a novel catamaran Floating Offshore Wind Turbine (FOWT) concept and a numerical assessment of its dynamic characteristics subject to operational conditions when operating in 150 m water depth. A numerical tool, F2A, which couples FAST and ANSYS AQWA numerical tools via a Dynamic Link Library (DLL) is used to conduct efficient aero-hydro-servo-elastic simulations. The tool enables fully coupled time-domain simulations to predict the hydrodynamic loads, mooring tensions (using AQWA) and aero-elastic loads (using FAST) which is required for the complete evaluation of a FOWT's dynamic behaviour and performance. A verification study is conducted by comparing the catamaran FOWT's inherent characteristics against the ITI Energy barge FOWT. Furthermore, validation of the numerical results is achieved through comparisons with published results of similar models. More specifically, performance indicators of wind turbine platforms including dynamic responses, stability, and power production under operational conditions. It has been observed that the catamaran concept has significantly reduced responses (22 % and 7 % reduction in F-A tower-base bending moment and rotor thrust, respectively) and improved stability (50 % reduction in pitch response (RAO)) compared to the barge. The catamaran concept offers steady production in a full range of operation conditions. This research confirms that a catamaran floating support platform offers a viable alternative to existing support FOWT concepts for application in intermediate water and provides greater insight into the behavior of barge-type FOWT concepts.

* Corresponding Author (m.b.bashir@ljmu.ac.uk)

1. Introduction

The offshore wind industry is rapidly growing, stimulated by the urgent need to produce electricity from clean and sustainable energy sources. The demand for renewable energy has been one of the motivations for the recent upsurge in research on Floating Offshore Wind Turbines (FOWTs). The offshore environment offers attractive advantages over the onshore environment for wind power generation which include resource availability and stability, optimum wind speeds, relatively low wind shear and turbulence intensity, and increased probability of higher energy density (Liu et al., 2021).

Offshore wind now comprises of two industries which are based on whether the foundation, used to support the wind turbine, is fixed to the seabed or floating. Most existing offshore wind farms are in shallow waters and employ fixed-bottom foundation technology e.g., monopile, to support the wind turbine. However, as viable nearshore sites become exhausted future wind farms will inevitably have to move further from shore into deeper waters (Loughney et al., 2021). Economically, fixed-bottom structures do not represent practical solutions for wind turbine applications in water depths greater than 60 m (Goupee et al., 2014). Consequently, floating platforms have become the favoured option for supporting wind turbines in deep waters, hence the major research focus on FOWTs in recent years. (Yang et al., 2021).

There are four distinct FOWT groups which are classified based on their rotational (pitch and roll) hydrostatic stability characteristics, see **Figure 1** (Jonkman and Matha, 2011) (Thiagarajan and Dagher, 2014).

Spars are simple cylindrical structures with excellent hydrodynamic stability owing to its deep draught and low center of gravity (Meng et al., 2020). On the other hand, the draught of the spar is a constraint whereby the minimum water depth for application is restricted (Zheng et al., 2020). Hywind Scotland, developed by Statoil (now Equinor) (Equinor, 2020) was the world's first fully operational floating offshore wind farm. The farm consists of five 6 MW wind turbines using spar platforms.

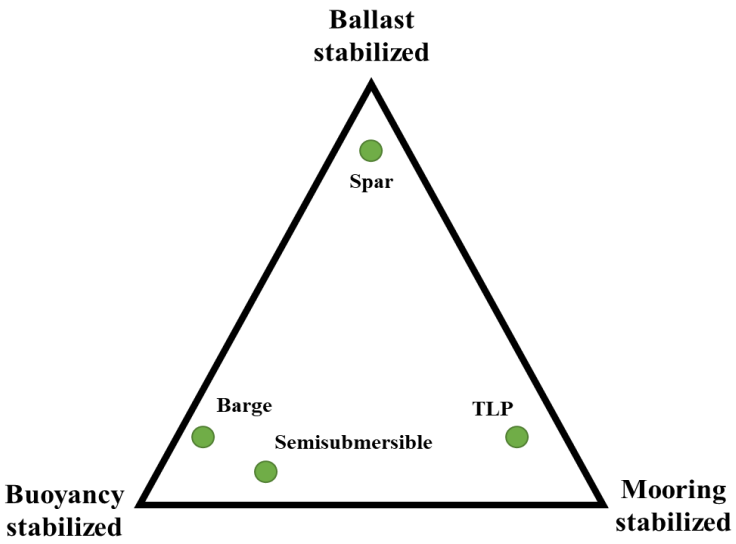

Figure 1. Stability triangle with annotation of common floating offshore wind types (Thiagarajan and Dagher, 2014).

A Tension-Leg Platform (TLP) uses a mooring system of taut vertical tendons to keep the platform upright and in position. The platform has excessive positive buoyancy which keeps the tendons constantly taut. TLPs are typically smaller structures geometrically compared to the other types (Taboada, 2016) and has good potentials for application due to its limited motions derived from the mooring system. (Murfet and Abdussamie, 2019). Despite these positives, the costs, and risks of application of a TLP remain relatively unknown unless full-scale sea testing is conducted.

Semisubmersibles and barge platforms are stabilized through buoyancy by taking advantage of their large waterplane areas. Semisubmersibles are usually composed of several columns connected to each other through braces or pontoons. The hydrodynamic behavior of semisubmersibles subject to wind load excitations is considered particularly good. Application of this platform type is deemed to be more achievable due to ease and tendency to have lower costs in their installation (Shi et al., 2019). However, the construction is more difficult despite the ability to be fabricated at dockside. Furthermore, the design of semisubmersibles is far more challenging due to complexity in their dynamic responses, caused by the combined effects of wind-wave coupled loads. More specifically, it is the heave response of this platform type which is a cause of concern because of its influence on general platform stability (Liu et al., 2016). Three 8.4 MW semisubmersible FOWTs developed by Principle Power (Principle Power, 2020) are in full operation off the coast of Portugal as part of the WindFloat Atlantic project.

These platforms are currently the largest FOWTs in the world with power generated capacity that can supply up to 60,000 users each year.

Barge platforms possess good advantages in their fabrication, assembly, deployment and anchoring when compared to other platform types. They have simple geometry, and a wind turbine can be easily mounted onto a barge dockside and the entire assembly can be towed by tugboats to site. This operation can eliminate any need for specialist vessels. Such operations mean barges have lower overall costs of fabrication and installation compared to the others. However, the uptake of barge platforms for intermediate water application is limited by problems that include its sensitivity to pitch stability in waves, high tower-base bending moments (Jonkman and Matha, 2011) and complex requirements for its operational control (Olondriz et al., 2018). Although the ITI Energy barge concept has been around for a while, the only high capacity barge FOWTs in operation are the Ideol demonstrators of its Damping Pool concept, Floatgen (Ideol, 2020a) and Hibiki (Ideol, 2020b), off the coasts of France and Japan, respectively. Each platform type has its own advantages and disadvantages and as the floating wind industry is still in an early stage there is a lack of consensus on which FOWT type performs best. This often means the simplest method to improve on platform dynamics is a redesign of the floater. Therefore, this paper proposes a novel catamaran-type FOWT concept.

Catamarans are widely used in the maritime transportation and leisure industries (Fang et al., 1997) and have been adopted to build the largest construction vessel in the world (Allseas, 2021) and green power boats such as ECO SLIM (Drassanes Dalmau, 2021). Catamarans are renowned for their good stability and large usable deck areas, both of which are beneficial for offshore renewable energy platforms. The deck area can be used to enhance safety when carrying out operation and maintenance work and utilized to support infrastructure for other functions such as ocean energy generation, solar panels, and hydrogen generation. Within the context of marine vehicles, vessel stability is governed by transverse stability (roll). A catamaran primarily depends on its beam (width) and demi-hull buoyancy for heeling stability. This means that the wider the beam and longer the dimensions, the greater the stability. These features help catamarans resist rolling to one side because the other hull's buoyancy overcomes the force of the rising or falling sea. For a FOWT, its longitudinal stability (pitch) can be

considered an important criterion in design as it directly affects the generated power quantity (Johlas et al., 2021). Typically, the longitudinal stability of a marine vessel is greater than its transverse, hence the reason for emphasis on transverse stability on the safety aspects of vessels in ship research (Dzan et al., 2013). Based on this, there is good possibility that modifying a catamaran into a FOWT support platform has worth because of their renown transverse stability. Moreover, there have been some studies on converting a conventional catamaran into a tidal energy platform (Qasim et al., 2018), (Junianto et al., 2020), (Brown et al., 2021). There is a lack of literature that attempt to modify a catamaran into a suitable support platform for wind turbine operations which presents the opportunity for research and incentive for this investigation.

To conduct feasibility studies, advanced numerical tools are required which enable the analysis, optimization, and preliminary design of FOWTs for a variety of configurations so that the technical and economic feasibility can be determined. Jonkman (2009) presented FAST, now known as OpenFAST due to its open-source nature, which is a framework that couples numerical codes capable of modelling aerodynamics, hydrodynamics for offshore structures, control and servo dynamics and structural dynamics to enable fully coupled time-domain simulation of FOWTs. OpenFAST is one of the most widely adopted numerical tools used to evaluate wind turbines. Barooni et al. (2018) presented the development of an open-source numerical model to enhance understanding of governing equations of a fully coupled nonlinear FOWT. In order to strengthen simulation capabilities of existing numerical tools for the FOWT design, Yang et al. (2020) published research on the development of a coupling framework called FAST2AQWA (F2A). F2A couples two well-known analysis tools via a dynamic link library to create a superior numerical tool for predicting nonlinear dynamics of a FOWT subject to wind, wave, and current loadings.

In this preliminary development of a novel catamaran-type FOWT concept the hydrodynamic characteristics and dynamic responses are numerically investigated using F2A for a range of operational load cases in intermediate water depth. An evaluation of the FOWT's dynamic behaviours and performance is carried out following the prediction of dynamic responses. A verification study has been conducted by comparing the catamaran concept developed in this study with a conventional barge

platform known as the ITI Energy barge. The results of the comparison are required for validation purposes and as part of the feasibility of the catamaran design. The results also provide insight into how the catamaran FOWT performs against another platform of a similar capacity. Thus, this paper is organized as follows: a description of the models is detailed in Section 2. Section 3 introduces the numerical tool used to analyze the FOWT systems in this research. Load cases and validation is discussed in Section 4, and results and discussion are presented in Sections 5 and 6. Conclusions are drawn in Section 7.

2. Model descriptions

This study uses the NREL 5 MW reference wind turbine (properties given in **Table 1**) to assess the capability of the proposed concept to function as a FOWT. The wind turbine is a conventional three-bladed horizontal-axis, upwind variable-speed wind turbine and comprises of blades, hub, nacelle, and tower. The main components of the FOWT system are the following: (1) wind turbine, (2) floating platform, and (3) mooring system.

Table 1. Properties of NREL 5 MW Reference Wind Turbine.

Parameter (Units)	Value
Rated Power (MW)	5
Rotor & hub diameter (m)	126 & 3
Cut-in, rated, cut-out wind speed ($m \cdot s^{-1}$)	3, 11.4, 25
Hub height (from the bottom of the tower) (m)	90
CM (Centre of Mass) location (from bottom of the tower) (m)	64
Rotor mass (kg)	110,000
Nacelle mass (kg)	240,000
Tower mass (kg)	347,460
Total mass (including tower) (kg)	697,460

The proposed concept is inspired by a typical catamaran vessel with a large deck mounted atop two equally spaced demi-hulls. The wind turbine is situated in the middle of the platform so that the tower centreline and platform centreline align and pass through the origin (0, 0, 0). As a preliminary design, the dimensions of the catamaran platform were selected so that the volume and displacement are similar to a barge platform. Any improvement or deterioration in performance would therefore be attributable to the platform design.

145 The barge FOWT model used for benchmarking and verification in this study is the ITI Energy
146 barge, a preliminary barge concept developed by the Universities of Glasgow and Strathclyde, and ITI
147 Energy. Further details of the platform can be found in (Jonkman, 2007).

148 To prevent drifting from installed location, each floating platform is moored by a system of eight
149 slack, catenary lines. For both platforms, at every bottom corner two mooring lines connect to the
150 platform separated by a 45° angle. The properties of the floating platforms are listed in **Table 2** and the
151 mooring system properties are given in **Table 3. Figures 2 & 3** present the CAD model of the catamaran
152 floating platform labelled with appropriate dimensions and the mooring system configurations of both
153 platforms created in ANSYS AQWA.

154 **Table 2.** Platform Properties.

	Catamaran	**ITI Energy barge**
Diameter or width × length (m), (LOA = length overall) (m)	45 × 60, (LOA = 77.3)	40 × 40
Space between demi-hulls (m)	25	-
Draught (m)	4	4
Elevation to platform top (tower base) above SWL (m)	6	6
Total volume (m^3)	15,684	16,000
Water displacement (m^3)	5,480	6,400
Mass (kg)	4,901,080	5,452,000
CM location (m)	(0, 0, 1.51)	(0, 0, -0.2818)
Roll inertia about CM (kg m^2)	4,672,683,194	726,900,000
Pitch inertia about CM (kg m^2)	6,800,310,371	726,900,000
Yaw inertia about CM (kg m^2)	11,190,569,096	1,454,000,000

155

156 **Table 3.** Mooring System Properties.

	Catamaran	**Barge**
Number of mooring lines	8	8
Depth to fairleads & anchors (m)	4 & 150	4 & 150
Radius to fairleads & anchors (m)	42.436, 429.095 & 439.566	28.28 & 423.4
Section length (m)	474.1	473.4
Mooring line diameter (m)	0.0809	0.0809
Line mass density (kg m^{-1})	130.4	130.4
Line extensional stiffness, EA (N)	589,000,000	589,000,000

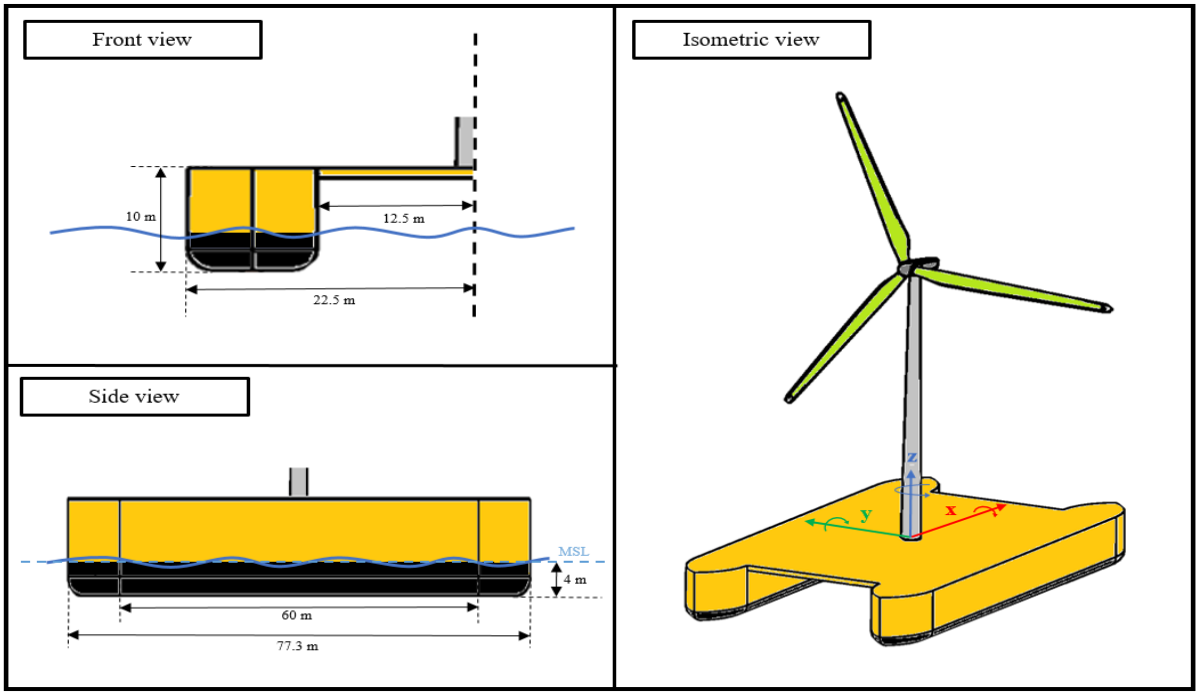

Figure 2. Preliminary catamaran FOWT concept schematics.

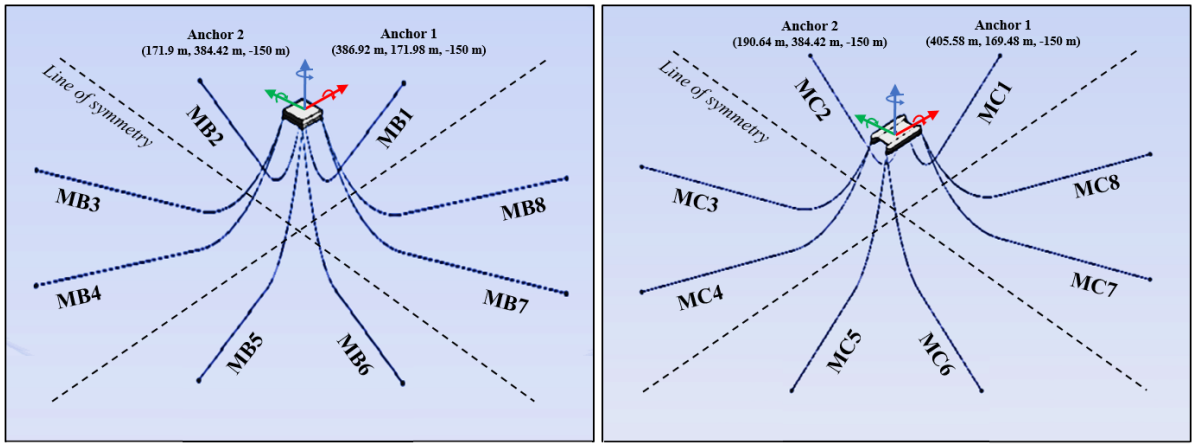

Figure 3. Mooring system configurations in ANSYS AQWA: barge (left), catamaran(right).

157

158 **3. Theoretical background and numerical modelling framework**

159 **3.1 Linear potential flow theory**

160 External flows around bodies can be represented by linear potential flow theory. For a bluff body
161 in waves, its radiation and diffraction problems must be solved to obtain the hydrodynamic coefficients
162 required for subsequent analysis of its dynamic behaviours. Application of potential flow theory is done
163 based on the assumption that the fluid is irrotational (without vorticity), incompressible (constant

density), and inviscid (zero viscosity). The fluid field velocity around the floating body is calculated once the velocity potential, ϕ, as a function of spatial displacement x, y, z and time, t and the relevant boundary conditions satisfy the conservation of mass and momentum conditions. The velocity potential equation must also satisfy the Laplace equation (Eq. 1):

$$\nabla^2 \phi = 0 \quad [1]$$

The total velocity potential induced by fluid flow around the body is expressed as a combination of incident wave, diffraction (incoming waves would scatter due to existence of floating body) and radiation (waves are radiated due to structure motions). This is represented by (Eq. 2):

$$\phi(x, y, z; t) = \phi_I(x, y, z; t) + \phi_D(x, y, z; t) + \phi_R(x, y, z; t) \quad [2]$$

$$\phi_R(x, y, z; t) = \sum_{k=1}^{6} \zeta_k \phi_{R_k}(x, y, z; t) \quad [3]$$

where $\phi_I(x, y, z; t)$ is the incident wave component of velocity potential in space and time, $\phi_D(x, y, z; t)$ is the spatial diffraction wave potential as a function of time, $\phi_R(x, y, z; t)$ is the radiation potential also in space and time. $\phi_{R_j}(x, y, z; t)$ is the radiation potential of the floating body induced by the platform movement in the k-th mode, ζ_j represents the platform's displacement in the k^{th} mode under the action of a unit wave amplitude, and $k = 1,2 \ldots,6$ represents the floating body's six degrees of freedom (surge, sway, heave, roll, pitch, and yaw).

Detailed representation of the incident wave potential $\phi_I(x, y, z, t)$ is given in equation (Eq.4) as:

$$\phi_I(x, y, z, t) = \frac{-iga}{\omega_0} e^{k_0 z} e^{i(k_0 x cos\theta + k_0 y sin\theta - \omega_0 t)} \quad [4]$$

where i is the imaginary unit component of the incident wave, a is the unit incident wave amplitude, gravitational acceleration is represented by g, while k_0 is the wave number, and θ is the incident wave angle.

When the wave velocity potentials are known, the first-order hydrodynamic pressure distribution may be calculated using the linearized Bernoulli equation given in (Eq.5).

$$p = -\rho \cdot \frac{\partial \phi(x,y,z,t)}{\partial t} \quad [5]$$

Following the prediction of the water pressure distribution, the various fluid forces may be obtained by integrating the pressure over the wetted surface of the body.

The first order hydrodynamic force and moment components can be represented in a generalized form:

$$F(x,y,z;t) = \iint_S p \cdot n_j(x,y,z;t)dS = = -i\omega\rho \iint_S [\,\phi(x,y,z;t)] \cdot n_j(x,y,z;t)dS \quad [6]$$

where ρ is the seawater density (kg/m^3), S is the floating body's wetted body surface area (m^2), and n_i is the wetted body surface's normal vector in the j-th mode.

From (Eq. 2) and (Eq.3), the total first order hydrodynamic wave force can be written as:

$$F_j = \left[\left(F_{I_j} + F_{D_j}\right) + \sum_{k=1}^{6} \zeta_k F_{R_{jk}}\right] \; where\; j = 1,6 \quad [7]$$

where (Eq.8) defines the j^{th} Froude-Krylov force, F_{I_j}, due to incident wave:

$$F_{I_j} = -i\omega\rho \iint_S [\,\phi_I(x,y,z;t)] \cdot n_j(x,y,z;t)dS \quad [8]$$

(Eq.9) defines the diffracting force, F_{D_j}, due to diffraction:

$$F_{D_j} = -i\omega\rho \iint_S [\,\phi_D(x,y,z;t)] \cdot n_j(x,y,z;t)dS \quad [9]$$

(Eq.10) defines the radiation force, $F_{R_{jk}}$, due to the radiation wave induced by the k^{th} unit amplitude body rigid motion:

$$F_{R_{jk}} = -i\omega\rho \iint_S [\,\phi_{R_k}(x,y,z;t)] \cdot n_j(x,y,z;t)dS \quad [10]$$

The hydrodynamic wave force can be further characterized in terms of active and reactive components. The active force, or the exciting force, is the combination of the Froude-Krylov force and

196 diffraction force. The reactive force is the radiation force due to the radiated waves induced by body
197 motions.

198 If the radiation wave potential is expressed in terms of real and imaginary parts, then the added
199 mass and radiation damping coefficients can be obtained:

$$\begin{aligned} F_{R_{jk}} &= -i\omega\rho \iint_S \{Re[\,\phi_{R_k}(x,y,z;t)] + iIm[\phi_{R_k}(x,y,z;t)]\} \cdot n_j(x,y,z;t)dS \\ &= \omega\rho \iint_S Im[\,\phi_{R_k}(x,y,z;t)] \cdot n_j(x,y,z;t)dS \\ &\quad - i\omega\rho \iint_S Re[\phi_{R_k}(x,y,z;t)] \cdot n_j(x,y,z;t)dS \\ &= \omega^2 A_{jk} + i\omega B_{jk} \end{aligned} \quad [11]$$

$$A_{jk} = \frac{\rho}{\omega} \iint_S Im[\phi_{R_k}(x,y,z;t)] \cdot n_j(x,y,z;t)dS \quad [12]$$

$$B_{jk} = -\rho \iint_S Re[\phi_{R_k}(x,y,z;t)] \cdot n_j(x,y,z;t)dS \quad [13]$$

200 where A_{jk} is the added mass coefficient, and B_{jk} is the damping coefficient (Lin and Yang, 2020).

201 **3.2 FAST2AQWA tool**

202 A newly developed aero-hydro-servo-elastic coupled tool is adopted in this study to predict the
203 coupled dynamic responses of the FOWTs induced by operational wave and wind climates. The tool is
204 based on the integration of an aero-servo-elastic solver, FAST (Jonkman and Buhl Jr, 2005) into a
205 commercial hydrodynamic analysis software tool, AQWA (ANSYS, 2012). F2A enables fully coupled
206 nonlinear aero-hydro-servo-elastic simulation to be conducted in the time domain. The new tool
207 operates by replacing the hydrodynamic module in FAST, known as HydroDyn, with AQWA to
208 calculate the hydrodynamic loads of a FOWT. The justification for the choice of F2A is that it uses the
209 superior predictive capabilities of AQWA to calculate the hydrodynamic loads acting on the FOWT.
210 FAST simulation capabilities are implemented within the coupled tool F2A via a coupling framework
211 to synchronously calculate the effects of wind induced loads and hydrodynamic forces. The coupling
212 of F2A is achieved through the user_force64.dll interface, which is a built-in Dynamic Link Library
213 (DLL) of AQWA for external force calculation. The coupling framework is represented by a flowchart
214 presented in **Figure 4** (Yang, 2020).

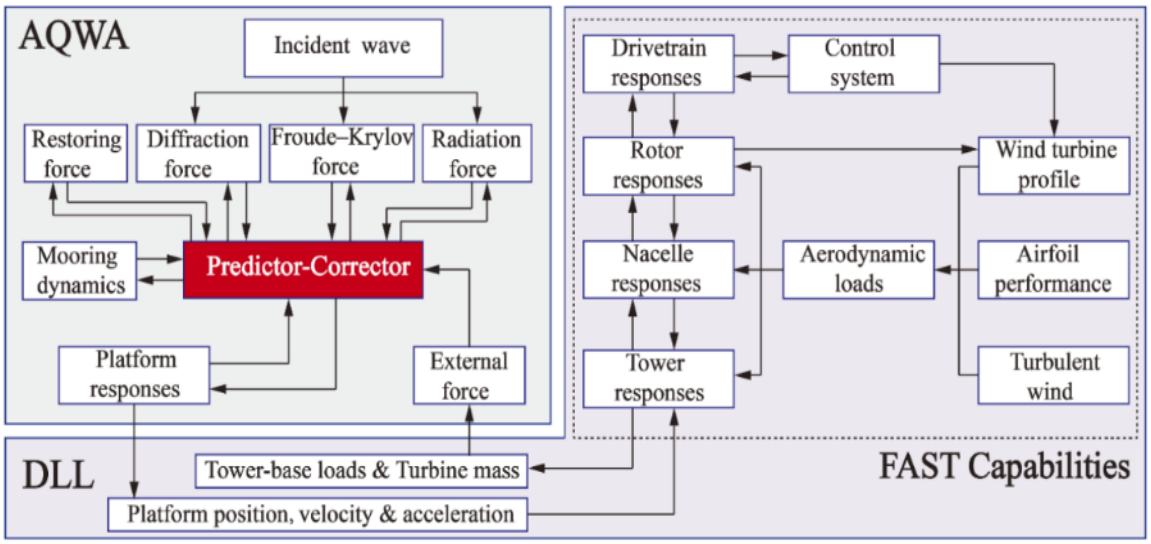

Figure 4. Flowchart of F2A (Yang, 2020).

It can be seen in **Figure 4** that the dynamic responses of a FOWT are predicted in different modules. More explicitly, the upper structures of the wind turbine (tower, rotor, and nacelle) are modelled in FAST, and the coupled dynamic responses are predicted within the DLL considering the platform kinematics obtained in AQWA. The terms within both AQWA and FAST are transformed to coincide with the platform's local coordinate system from their respective inertial coordinate systems before being fed into the DLL. This transformation becomes necessary to enable FAST to correct the kinematics of FOWT's upper structures in relation to its platform responses calculated in reference to its local coordinate system. Therefore, a transformation is needed as the platform responses predicted by AQWA are referred to its inertial coordinate system. Following successful transformation of the coordinate system, the platform's tower-base loads are subsequently calculated by FAST subroutines. The lower structure of the FOWT, which consists of the platform and mooring lines, is modelled in AQWA. The resulting dynamic responses, mainly hydrodynamic, are calculated in AQWA by solving the equation of motion of the platform using the calculated tower-base loads as an external force. The governing equation of motion of the platform is defined in (Eq.14):

$$(\boldsymbol{M}+\boldsymbol{A})\ddot{x}+\boldsymbol{B}_{ext}\dot{x}+\boldsymbol{B}_2\dot{x}|\dot{x}|+\int_0^t \boldsymbol{h}(t-\tau)\dot{x}(\tau)d\tau+\boldsymbol{C}x=\boldsymbol{F}_{ext} \quad [14]$$

where $\boldsymbol{M}$ is the inertial mass matrix, $\boldsymbol{A}$ is the added mass matrix, and $x, \dot{x}, \ddot{x}$ are the unknown FOWT platform's displacement, velocity, and acceleration vectors, respectively, for each degree of freedom. $\boldsymbol{B}_{ext}$ and $\boldsymbol{B}_2$ are the linear and quadratic viscous damping coefficients respectively, typically obtained from model tests, $\boldsymbol{h}(t)$ is the radiation impulse function defined by

$$\boldsymbol{h}(t) = \frac{2}{\pi}\int_0^{\infty} \boldsymbol{B}_{Pot}(\omega)\cos(\omega t)\, d\omega \qquad [15]$$

where $\boldsymbol{B}_{Pot}(\omega)$ is the potential damping matrix corresponding to the wave frequency of ω, and $\boldsymbol{C}$ is the stiffness matrix with contributions from hydrostatic and the mooring line restoring forces. Matrix $\boldsymbol{A}$ and $\boldsymbol{B}_{Pot}$ can be computed numerically using the potential theory-based solver. in AQWA. This, in turn, can provide the total external force vector denoted by $\boldsymbol{F}_{ext}$. For more information on the F2A coupling framework and coordinate system transformations refer to (Yang et al., 2020).

4. Simulation

4.1 Load cases and environment

Table 4 details the several types of analysis carried out and Load Case (LCs) conditions simulated. The first set of analyses focuses on system identification, including frequency-domain analysis to obtain hydrodynamic coefficients, free-decay simulations to find natural frequencies, hydro-elastic response with regular waves in absence of wind, and RAOs for a complete assessment of hydrodynamic characteristics. The next set of simulations are fully coupled aero-hydro-servo-elastic time-domain simulations used to investigate the performance of the catamaran floating wind turbine system under combined wind and wave excitation. For these simulations, the met-ocean data used is from a site located off the north coast of Scotland. LC 1 – 7 are defined in accordance with IEC 61400-3 where U_w is the locations' turbulent wind speed, measured at FOWT's hub-height (m/s), H_s is the significant wave height (m) and T_p is the spectral peak period (s). The wind characteristics of the selected site are modelled as three-dimensional turbulent wind fields based on the Kaimal turbulence model for IEC Class C and using TurbSim, a sub-program in FAST (Jonkman and Buhl Jr, 2006). The site wave conditions are modelled as irregular waves using the Pierson-Moskowitz wave spectrum in AQWA.

Furthermore, the length of each simulation is 4,600 s, with the first 1,000 s discarded to remove transient effects potentially interfering with final results.

Table 4. Load Cases.

LC	Description	U_w [m/s]	H_s [m]	T_p [s]
HDC	Frequency-domain analysis to obtain hydrodynamic coefficients	-	-	-
FD	Free decay analysis	-	-	-
RW	Regular wave	-	2.1155	5.2555
RAO	Response amplitude operators (white-noise wave)	-	2	10
1	Cut-in	4	1.6146	3.4985
2	Below-rated	8	1.8037	4.2657
3	Rated	11.4	2.1155	5.2555
4	Above-rated	18	2.9585	7.1203
5	Cut-out	25	4.0257	8.8897
6	Rated (Wave Dir 30°)	11.4	2.1155	5.2555
7	Rated (Wave Dir 90°)	11.4	2.1155	5.2555

4.2 Validation

The novelty of the catamaran FOWT concept means that no experimental or numerical data, or benchmark model is available in public domain, yet the numerical model requires verification and validation for results to attain credibility. Consequently, the methodology used to verify the catamaran is based on a comparison of results of the ITI Energy barge model with published research. Good agreement between the results of the barge numerical model and published research reassures the credibility of this new concept by verifying the procedure to obtain the results. Following verification, the behavior of the catamaran model is validated through comparisons with published results of similar models.

5. Assessment of hydrodynamic characteristics

5.1 Hydrodynamic coefficients

The hydrodynamic coefficients of the catamaran and barge are calculated using ANSYS AQWA and presented in **Figures 5 & 6**. The coefficients are obtained in six degrees-of-freedom for a wave

frequency range of 0.05 – 4.0 rad/s at intervals of 0.05 rad/s and incident angles varying between 0 – 90° at intervals of 30°. The calculated hydrodynamic coefficients of the barge platform were validated against the results published by (Olondriz et al., 2018). Overall, there is good agreement between the results which ensures the 3D analysis method used to obtain the hydrodynamic coefficients for both platforms is accurate and reliable. However, there is some discrepancy for heave and yaw radiation damping coefficients. Concerning heave damping coefficient, the plots follows a similar trend, however the peak amplitude of the present numerical model occurs at a higher frequency to the published results and concerning yaw, the plots follow an identical trend however the curve does not fall as sharply as frequency increases. Next, the trend of the hydrodynamic coefficient plots of the catamaran follows a similar pattern to the hydrodynamic coefficients plots of three catamarans modelled by (Fang, 1996) and one catamaran modelled by (Wellicome et al., 1995). The successive occurrence of peaks at discrete frequencies is inherently a characteristic of catamaran vessels. The similarity in results provides additional reassurance that the model is behaving as expected.

Catamarans experience a phenomenon known as dynamic amplification which is caused by entrapped wave action between its demi-hulls. This phenomenon can lead to enhanced motion behaviours. A series of characteristic frequencies, ω_r , exist where demi-hull oscillation strongly excites the motion of the entrapped fluid; these frequencies can be identified by the following formula:

- Symmetric interaction: $\omega_r = \sqrt{2n\pi g/d_r}$ for n = 1, 2, 3 … [16]
- Antisymmetric interaction: $\omega_r = \sqrt{(2n-1)\pi g/d_r}$ for n = 1, 2, 3 … [17]

where d_r is the demi-hull separation (m).

The characteristic frequencies can be either separated into symmetric or anti-symmetric interaction. Symmetric interaction affects the vertical plane motions (surge, heave, pitch) and antisymmetric interaction affects the horizontal plane motions (sway, roll, yaw). These frequencies are analogous to the resonant modes of a standing wave between two vertical walls.(Fang, 1996). Moreover, the fact that catamarans have negative added mass in a stationary condition suggests that the effect of hydrodynamic interaction between the demi-hulls is strong. The frequency of the standing wave

295 depends on the distance between the demi-hulls. The wider the distance is between the demi-hulls, the
296 lower the frequency at which the phenomenon occurs (Dabssi et al., 2008).

297 In **Figures 5 & 6**, the characteristic frequencies are distinct. Using (Eq.16) and (Eq.17) to calculate
298 the characteristic frequencies, for heave and pitch plots of added mass and radiation damping
299 coefficients, small peaks occur at 1.57 rad/s due to symmetric interaction. For the added mass
300 coefficients, a smaller peak can be seen at a frequency of 2.22 rad/s. Peaks also exist for surge mode,
301 however due to the scaling of the axis, they are not visible.

302 For horizontal plane motions, peak responses occur at 1.11, 1.92, 2.48, 2.93, 3.33 and 3.68 rad/s
303 due to asymmetric interaction between the demi-hulls. Only the first two frequencies are dominant for
304 the added mass and radiation damping coefficients of sway, roll, and yaw motions. Similar to pitch, a
305 small peak occurs before the first characteristic frequency for roll. This peak corresponds to the roll
306 resonant frequency.

307 Comparison of hydrodynamic coefficients show that the catamaran exhibits lower surge and heave,
308 and higher sway, roll, pitch, and yaw added mass and damping coefficients. This observation suggests
309 that the platform has lower hydrodynamic restoring stiffness and potential damping for surge and heave
310 modes. At the same time, hydrodynamic restoring stiffness and damping for sway, roll, pitch, and yaw
311 modes are higher. Moreover, it is expected that the barge platform will be more sensitive to aerodynamic
312 loading due to smaller pitch coefficients, whilst the catamaran will be more sensitive to wave loading
313 as a result of smaller surge coefficients.

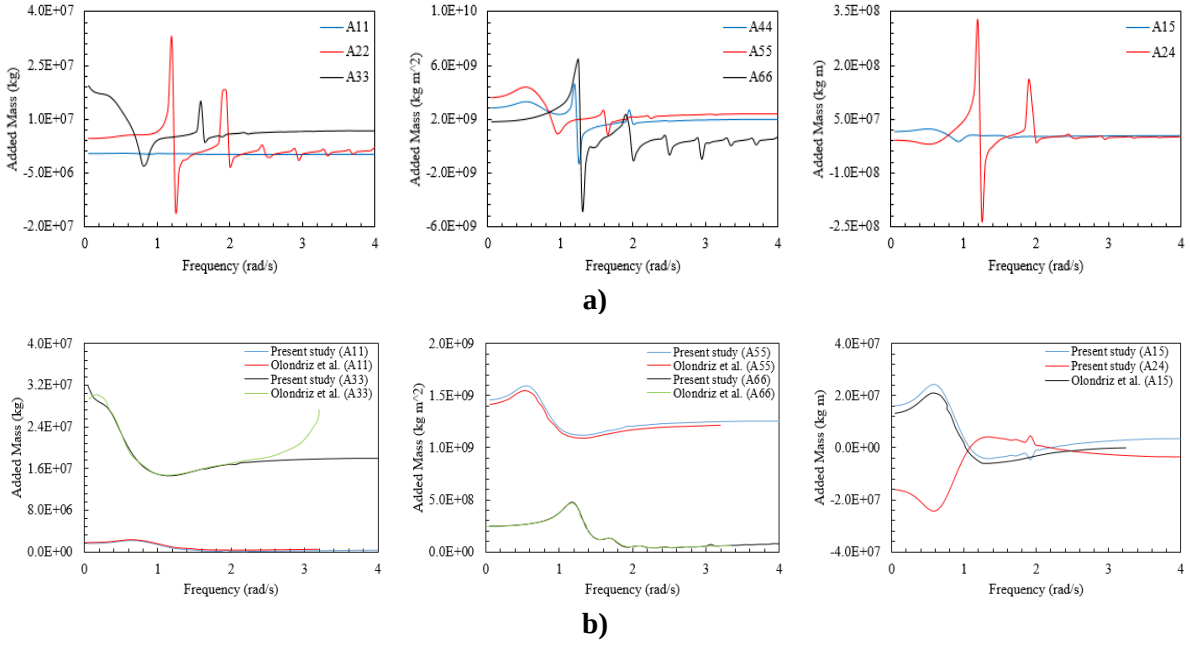

Figure 6. Hydrodynamic added mass coefficients a) catamaran b) barge.

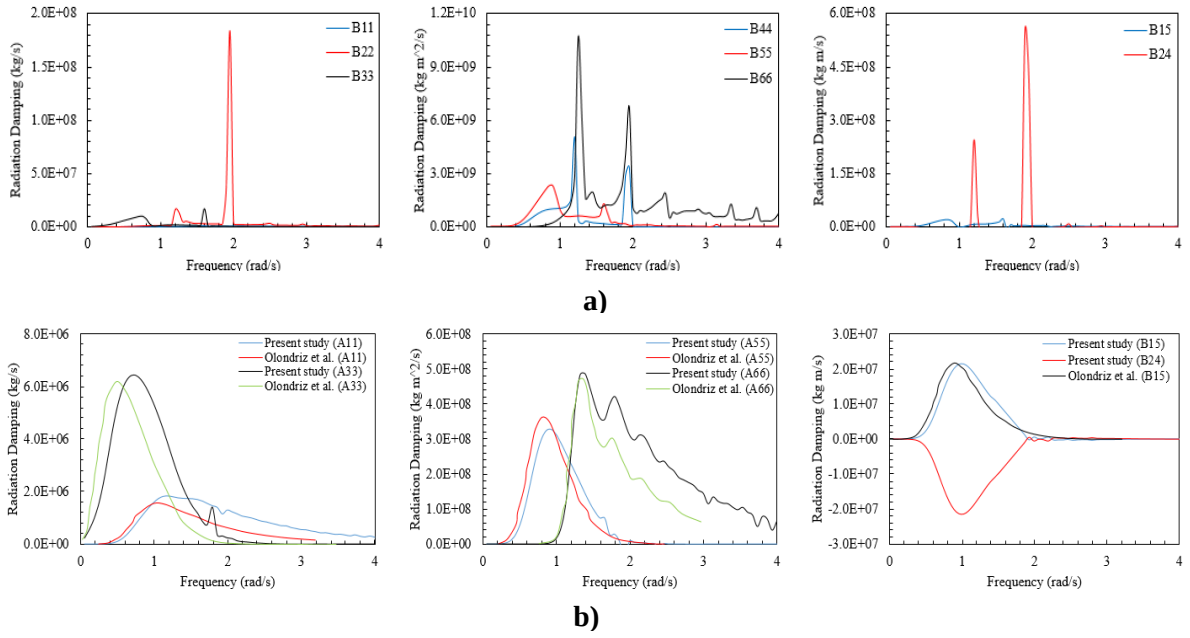

Figure 5. Hydrodynamic radiation damping coefficients a) catamaran b) barge.

5.2 Free decay

A free decay analysis was conducted for both platforms in six degrees of freedom. The natural periods of the platforms are presented in **Table 5** and plotted graphically in **Figure 7**.

Table 5. Natural periods (s) of the FOWT systems.

	Surge	Sway	Heave	Roll	Pitch	Yaw

Catamaran	121.6	157.1	5.4	10.6	9.8	109.5
Barge	137.7	137.7	7.1	11.8	11.8	52.5

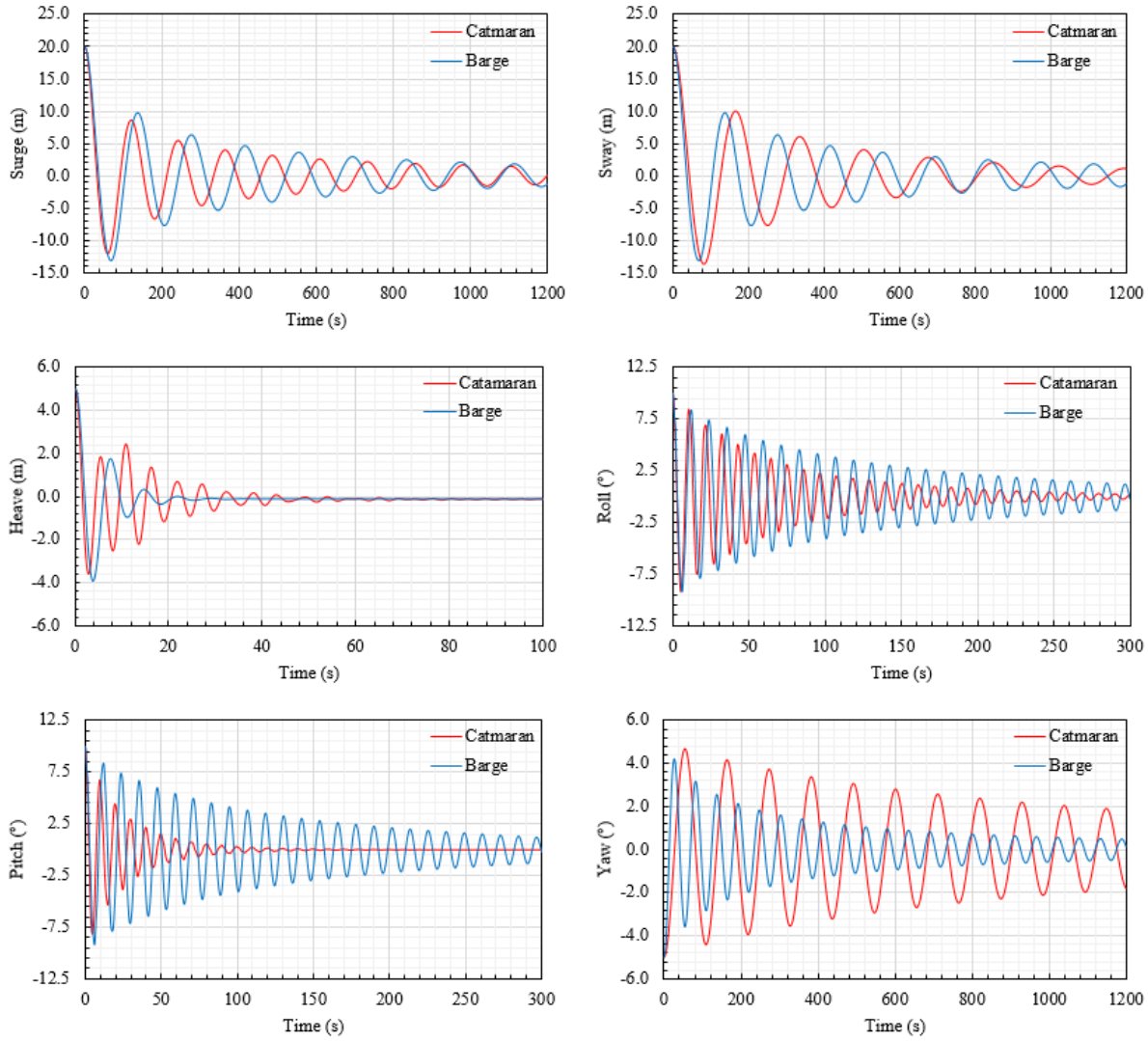

Figure 7. Free decay results.

5.3 Hydro-elastic response under regular waves

Figure 8 shows the time histories of platform surge, heave and pitch displacements, tower-top fore-aft displacement, tower-base force in the x-direction, and fairlead tensions (MB4/MC4) of both platforms subject to a regular wave with properties H = 2.1155 m and T = 5.2555 s. The results show the barge exhibits greater surge and pitch displacement, tower-top fore-aft displacement, tower-base force, and mooring line tension, whilst the catamaran has greater heave displacement.

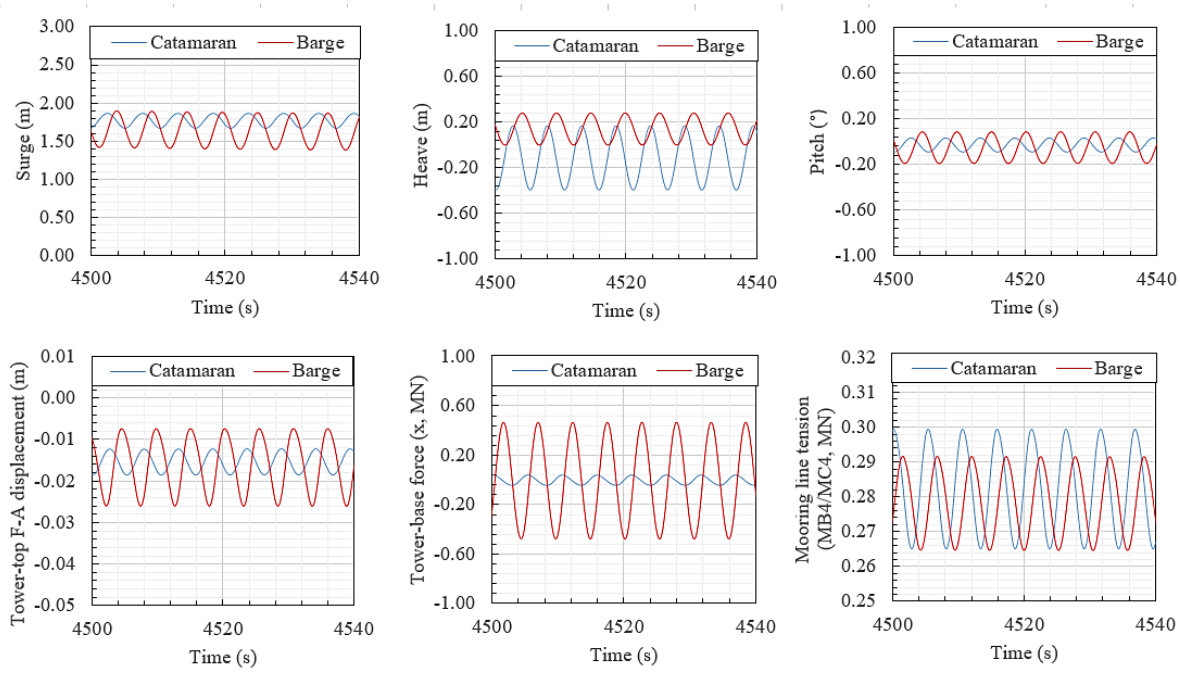

Figure 8. Hydro-elastic response with regular wave in absence of wind (H = 2.1155 m, T = 5.2555 s).

5.4 Response Amplitude Operators (RAOs)

Response Amplitude Operators (RAOs) are used in hydrodynamic analysis to initially assess the frequency-domain linear wave response of floating platforms (Robertson et al., 2014). In FOWT design, the hydrodynamic loads coupled with wind induced aerodynamics, structural dynamics, and servo-controller dynamics must be accounted in order to quantify their contribution and effects on platform responses (Aboutalebi et al., 2021). Simulations to predict the RAOs were performed in OpenFAST (National Renewable Energy Laboratory (NREL), 2021) with the process described in (Ramachandran et al., 2013) and (Aboutalebi et al., 2021). The RAOs for both catamaran and barge platforms are plotted in **Figure 9**. Similar to the methodology adopted in validating hydrodynamic coefficients, published numerical results for the RAOs of the barge exist; these have been used for validation. The RAO outputs in this study for the barge FOWT agree with the results published by (Aboutalebi et al., 2021).

RAOs are plotted for a frequency range of 0.1 – 1.25 rad/s and they show considerable excitation in surge, heave, and pitch modes. Since only wave response in a zero-degree heading was simulated, the responses for sway, roll and yaw are considerably less in magnitude due to the wave heading and absence of wind forcing.

Considering the surge mode, there is a shift in peaks from 0.52 rad/s to 0.62 rad/s. These peaks are attributable to the pitch resonant frequency of the corresponding platform. Furthermore, the catamaran RAO is slightly lower which suggests it is less responsive than the barge. The actual surge resonant frequency of both platforms occurs at a much lower frequency, hence why as frequency decreases the RAOs increase.

The heave RAO plots of both platforms are identical in the lower frequency range and follow the incident wave until approximately 0.4 rad/s. The RAO of the catamaran in the higher frequency range falls more sharply than the barge. However, at approximately 1.0 rad/s the barge RAO begins to level

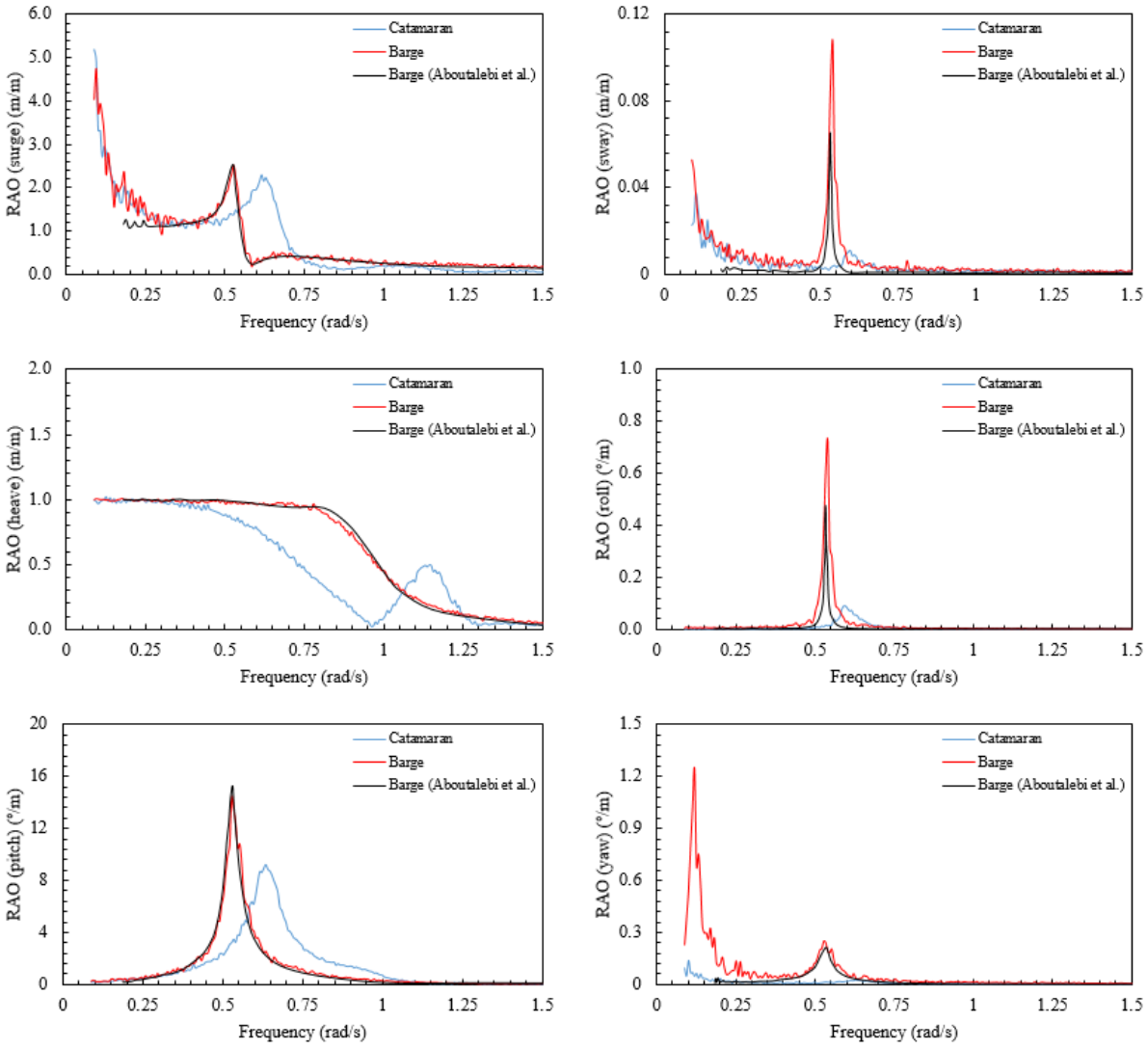

Figure 9. RAOs for 6 degrees of freedom of catamaran and barge platforms.

348 out whereas the catamaran experiences another peak. This peak corresponds to the frequency of the
349 standing wave created by the catamaran's demi-hulls.

350 For pitch mode, it is observed that the catamaran exhibits close to a 50 % reduction in response
351 compared to the barge. As mentioned above, the pitch resonance frequency of the catamaran is higher
352 than the barge. Also, the peak response of the catamaran has a wider band compared to the barge, which
353 means the catamaran is more responsive to a greater frequency range, whereas for the barge the peak
354 rises and falls more sharply.

355 ### 5.4.1 Varying angle of incidence wave

356 The RAOs of the catamaran platform for varying angles of incident wave are plotted in **Figure 10.**
357 These results aim to provide a better understanding into the behaviour of the platform subject to wave
358 misalignment.

359 The response of the platform in surge and sway are similar in magnitude of peaks and shape. The
360 largest response occurs in wave heading angles parallel to the direction of motion i.e., 0° for surge and
361 90° for sway, and the smallest response occurs in wave heading angles perpendicular to the direction of
362 motion i.e., 90° for surge and 0° for sway. For sway mode, a small peak occurs at approximately 1.3
363 rad/s for a wave heading angle of 90 °, this response is due to standing wave phenomenon between the
364 demi-hulls.

365 Considering the heave mode, in the frequency range 0.85 – 1.25 rad/s hydrodynamic interference
366 caused by the entrapment of wave between the two demi-hulls is prevalent. For a wave heading angle
367 of 90°, this phenomenon is most significant and has a maximum response of 1.8 m/m. At approximately
368 1.6 rad/s, another peak occurs which corresponds to the characteristic frequency for vertical plane
369 motions due to symmetric interaction.

370 Similarly, to surge and sway, roll and pitch follow the trend that the largest response occurs in wave
371 heading angles parallel to the direction of motion i.e. 0° for pitch and 90° for roll, and the smallest
372 response occurs in wave heading angles perpendicular to the direction of motion i.e. 90° for pitch and

0° for roll. One major difference is that the roll maximum amplitude is three times that of pitch; this is because the catamaran is vessel-shaped and when exposed to oblique waves significant rolling can be induced.

Considering yaw mode, for wave heading angles 0° and 90° there is insignificant response, and for 30° and 60° one peak and two peaks occur, respectively, explained by the characteristic frequencies for horizontal plane motion due to antisymmetric interaction.

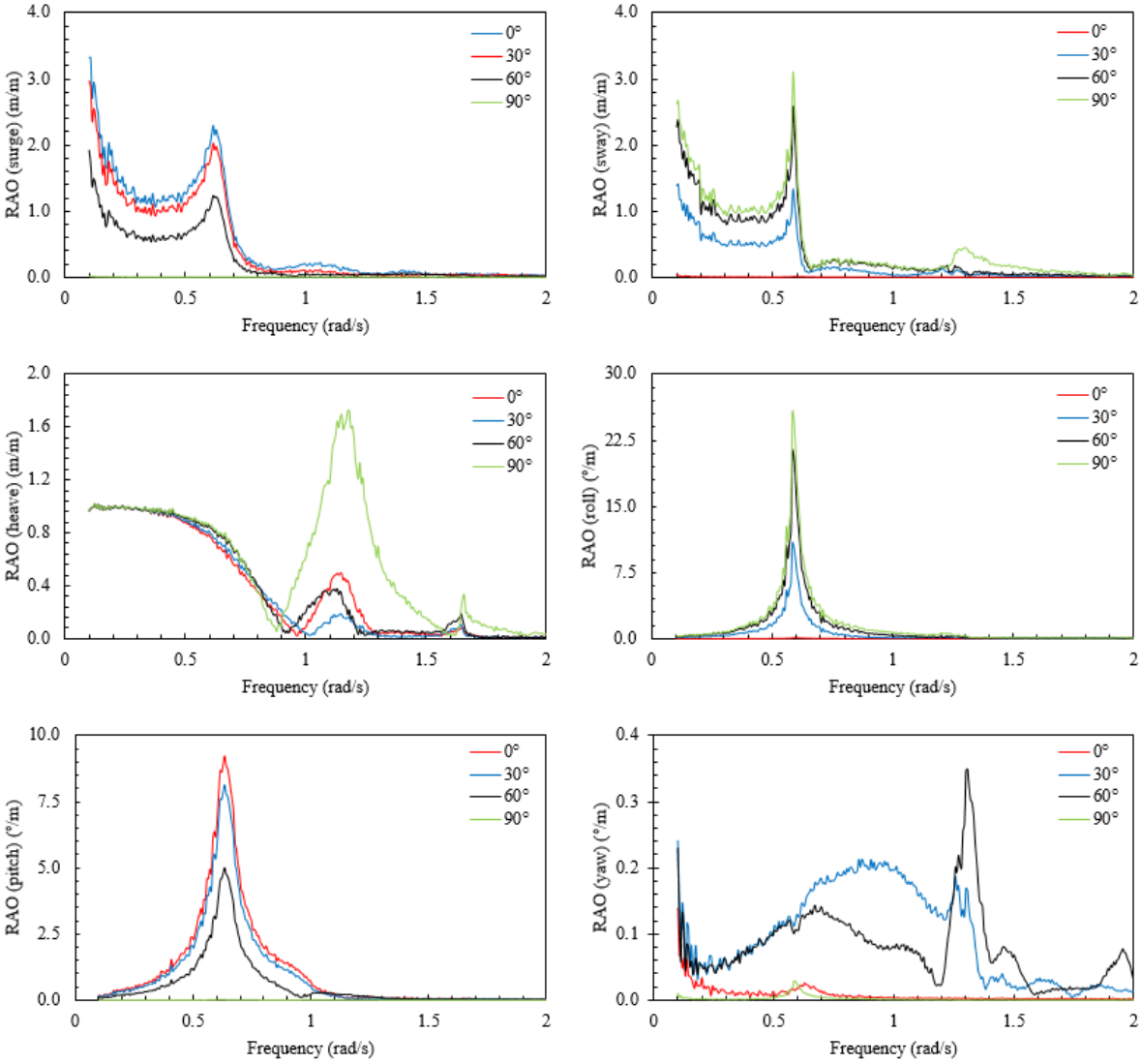

Figure 10. RAOs of catamaran for varying angle of incidence.

6. Dynamic Responses

6.1 Platform motions

The statistical motions of the two platforms are presented in **Table 6**. For LCs 1 and 2, the surge statistics are almost identical. Under LC 3, some differences are observed, it is predicted the catamaran has a smaller mean surge with greater fluctuation and a greater maximum surge. The highest mean surge for both platforms was predicted under LC 3, corresponding to the rated wind speed condition. A wind turbine operating at rated wind speed produces maximum rotor thrust (approx. 800kN for 5 MW wind turbine), which significantly influences the surge of FOWTs. Under LCs 4 - 5, the catamaran has a greater mean and maximum surge and increased fluctuation compared to the barge. Both platforms experience their greatest maximum surge under LC 5 because of the largest wave loads. For all five LCs, the heave statistics of the two platforms are indistinguishable apart from the maximum responses for the last 3 LCs. This was expected due to the comparable dimensions of the water plane areas. Considering pitch, for all LCs the catamaran platform has the smallest mean. The elongated geometry of the catamaran compared to the barge provides a greater restoring moment about the y-axis. The highest mean pitch response for both FOWTs is observed under LC 3. The fluctuation of the catamaran under LC 4 is noticeably greater compared to the barge. This is most likely due to combined wind and wave loading exciting the catamaran at its natural pitch period, nonetheless performance of the catamaran is good with a predicted mean pitch of 0.2° and maximum pitch of 8.52°.

Table 6. Statistical results of platform motion responses (1000 – 4600 s).

		Surge (m)		Heave (m)		Pitch (°)	
LC	Type	Catamaran	Barge	Catamaran	Barge	Catamaran	Barge
1	Max	16.96	**16.35**	**0.066**	0.300	**0.314**	1.025
	Mean	8.343	8.490	-0.125	**0.123**	**0.067**	0.328
	Std.dev	2.734	3.198	**0.059**	**0.059**	**0.080**	0.179
2	Max	34.68	**33.35**	**0.456**	0.645	**1.581**	2.153
	Mean	22.25	22.32	**-0.115**	**0.115**	**0.295**	1.094
	Std.dev	3.809	**3.674**	**0.114**	0.156	0.312	**0.226**
3	Max	48.14	**45.52**	**0.410**	1.149	**2.936**	3.826
	Mean	27.18	29.29	-0.143	**0.108**	**0.370**	1.726
	Std.dev	11.31	**7.050**	**0.151**	0.308	0.712	**0.545**
4	Max	44.41	**30.08**	**1.720**	2.148	8.519	**4.243**
	Mean	21.92	**19.30**	-0.134	**0.118**	**0.200**	0.997

	Std.dev	8.046	**4.298**	**0.398**	0.593	2.492	**1.026**
	Max	50.03	**37.19**	**2.727**	3.352	12.770	**12.190**
5	Mean	20.60	**8.583**	**-0.104**	0.122	**0.179**	0.862
	Std.dev	**10.78**	11.53	**0.733**	0.895	4.046	**3.775**

*(**BOLD** = minimum)*

6.2 Time- & Frequency-domain results

The time- and frequency-domain platform responses of both models under LC 3 are presented in **Figures 11** & **12**. Considering time-domain platform responses, it is obvious the catamaran has increased fluctuation from mean surge compared to barge. The mooring system is mainly responsible for surge stability, therefore in future research the mooring system is one aspect that will be further investigated. Considering heave, the stability of the catamaran is excellent, whilst the barge experiences greater fluctuation. The mean pitch of the catamaran is smaller compared to the barge; however greater variation is observed. Even with increased fluctuation, the maximum pitch of the catamaran does not exceed ±3°.

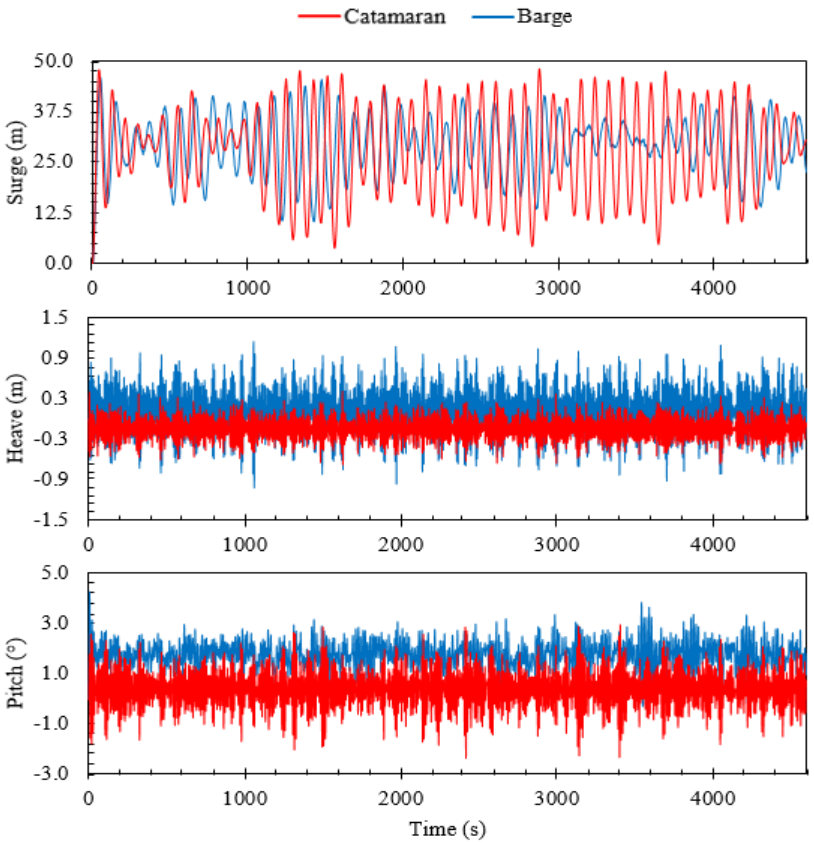

Figure 11. Time-domain responses of FOWT concepts under LC3 (rated wind speed).

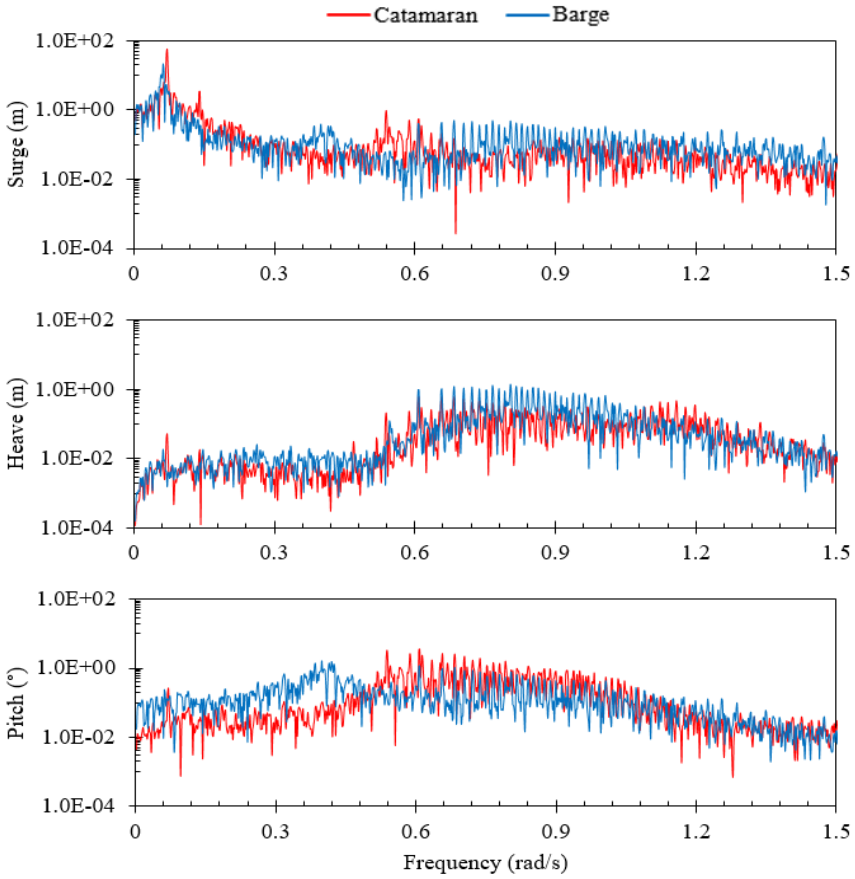

Figure 12. Frequency-domain (spectral) responses of FOWT concepts under LC3 (rated wind speed).

Considering frequency-domain platform responses, the amplitude of surge response in frequency-domain for the catamaran and barge platforms is dominant near 0.06 rad/s, corresponding to the resonant frequency of this mode for both platforms. Smaller peaks are observed at approximately 0.4 rad/s and 0.54 rad/s for the barge and catamaran, respectively, which equate to the pitch natural frequency of each platform. The response suggests the coupling between surge-pitch for both platforms is somewhat small. Concerning heave, there is a limited response in lower frequency region. Peaks occur at 0.80 rad/s and 1.14 rad/s, for the barge and catamaran, respectively, which is due to the heave natural frequency of the respective platform. Considering pitch, an obvious peak can be seen at approximately 0.4 rad/s, which corresponds pitch resonant frequency of the barge platform. The pitch resonant frequency of the catamaran platform is approximately 0.54 rad/s and the amplitude of the peak is slightly higher compared to the peak at resonant frequency of the barge.

6.3 Mooring line responses

Figures 13a) and **13b)** present the mean and maximum fairlead tensions of the two FOWTs. Both mooring system configurations use eight catenary lines to keep the platform in position. The symmetric nature of the mooring systems requires only certain mooring lines to be examined. Therefore, four mooring lines of the barge (MB1, MB3, MB5, MB7) and catamaran (MC1, MC3, MC5, MC7) mooring systems are selected. Due to incident waves, prevailing wind and rotor thrust all acting or travelling downstream, the fairleads upstream of the origin will experience the greatest tension. This is because such external forces cause the platform to drift downstream. As this happens, the mooring lines upstream will stretch increasing tension in the lines, in order to prevent drifting, whilst the mooring lines downstream will slack. Consequently, MB5 and MC5, exhibit the greatest tension. The barge and catamaran mooring lines have similar mean tensions under all LCs, except for mooring line MC5 in LCs 4 and 5 where MC5 is fractionally higher than MB5. Under these two LCs, the maximum tension of mooring line MC5 is approximately 1.5 times the tension of MB5 under LC4 and 2 times the tension

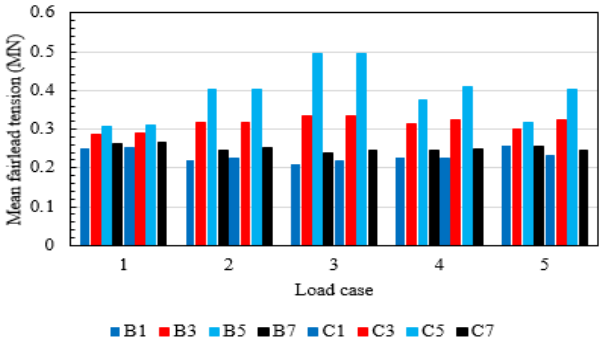

a) Mean fairlead tension.

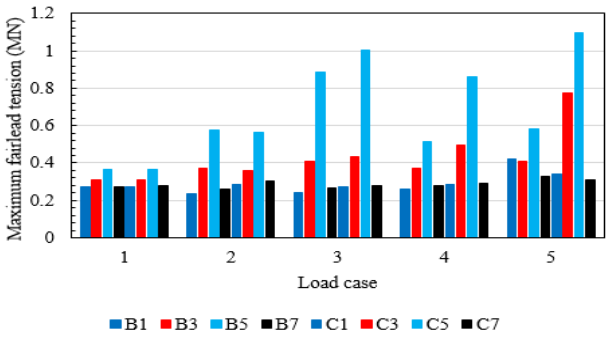

b) Maximum fairlead tension.

Figure 13. Fairlead tension (MB1 = barge line 1, MC1 = catamaran line 1).

under LC 5. This can be explained by the large surge response of the catamaran platform under these two LCs.

6.4 Power production

The generator power statistics for LC 1 - 5 are charted in **Figure 14** and the time-domain generator power under LC3 is presented in **Figure 15**. For LC 1 – 2, the results are incomparable. Under LC 3 - 5, the catamaran has greater maximum generator power but larger standard deviation, whilst the barge has greater minimum and mean generator power. In **Figure 15**, it can be seen both FOWTs follow similar trends for the entire simulation, however the barge has better quality power because of less fluctuation.

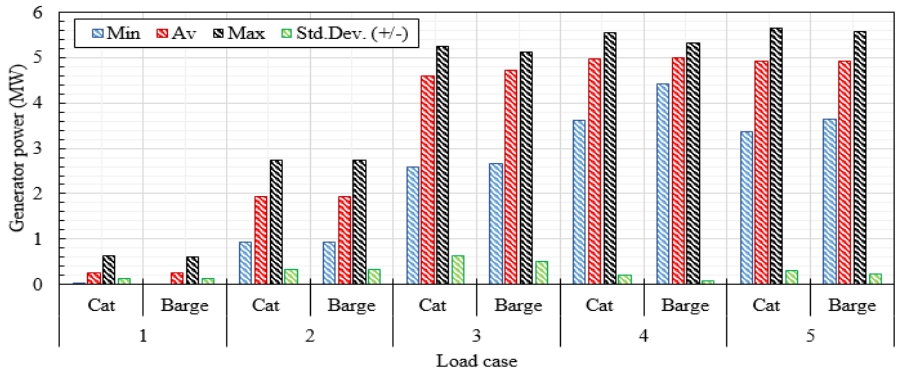

Figure 15. Comparison of generated power between catamaran and barge FOWTs.

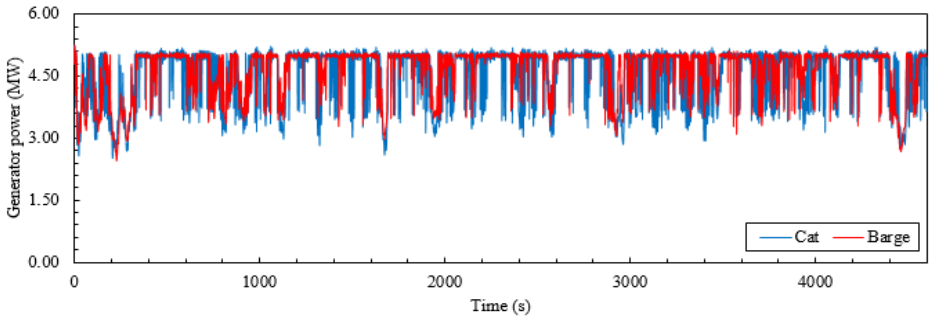

Figure 14. Generator power of the catamaran and barge FOWTs under LC3.

6.5 Blade, rotor, and tower responses

Figures 16 & **17**, plot the rotor thrust, Out-of-Plane (O-o-P) blade-tip deflection and tower-base bending moments of both platforms. Rotor thrust, O-o-P blade-tip deflection and Fore-Aft (F-A) tower-base moment all follow a similar trend because of the direct and indirect influence of the incoming wind. The rotor thrust, being the axial force, is applied by the wind kinematics on the wind turbine rotor and it is the dominant load acting on each FOWT. The O-o-P blade-tip deflection is the result of wind-induced force on the wind turbine blades. The F-A tower-base bending moment is mainly caused by the rotor thrust and has the most prominent influence on stress at the tower base. The peak thrust acting on both wind turbine rotors occurs under LC 3. This is also true for peak F-A tower-base bending moment and O-o-P blade-tip deflection. Comparing the two FOWTs, for all LCs, the barge platform has higher rotor thrust. Under LC 3, the barge and catamaran platforms have an approximate mean rotor thrust of 750 kN, and 700 kN, respectively, which is a difference of 7 %. The maximum rotor thrust of the barge and catamaran is 1066 kN and 1123 kN, respectively. The mean F-A tower-base bending moment is 64 MN·m and 52 MN·m for the barge and catamaran, respectively, representing a difference of 23 %. The

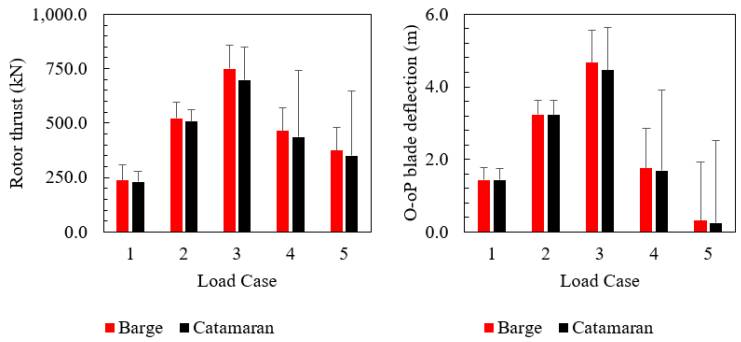

Figure 16. Comparison of mean rotor thrust and blade-tip deflection.

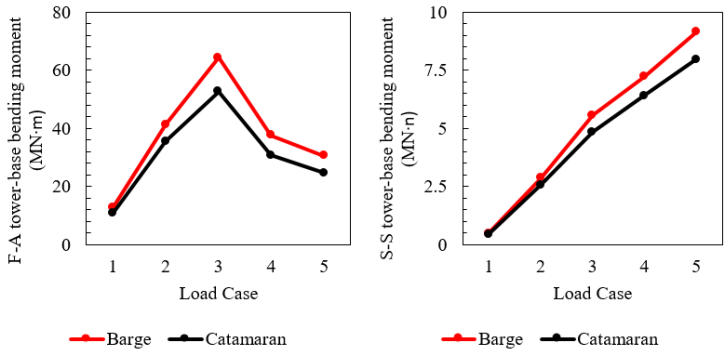

Figure 17. Comparison of barge and catamaran tower-base bending moments.

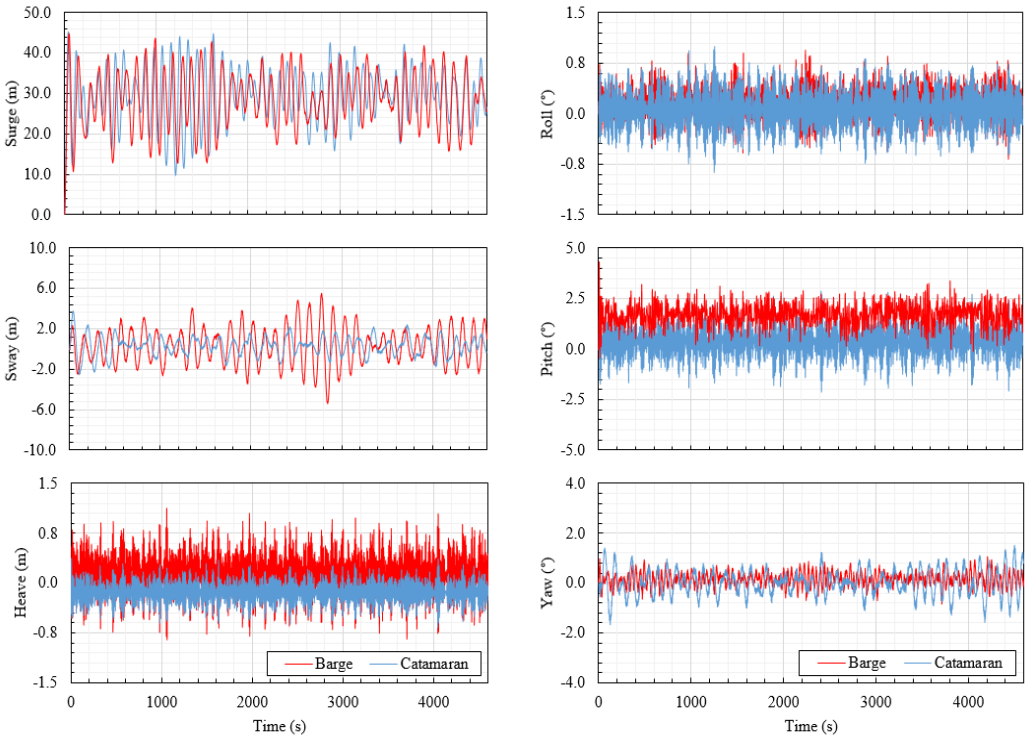

Figure 19. Time-domain platform motions under LC 6.

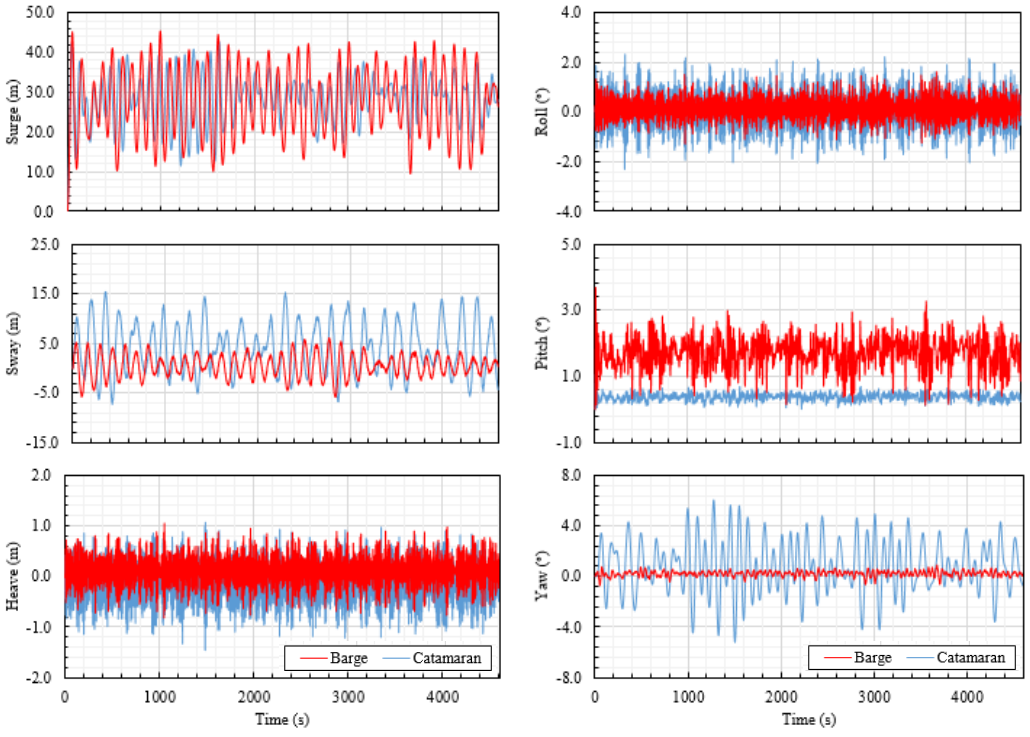

Figure 18. Time-domain platform motions under LC 7.

maximum F-A tower-base bending moment is 140 MN·m and 104 MN·m for the barge and catamaran, respectively. The mean O-o-P blade-tip deflection of both concepts for all LCs is similar. For LC 4 – 5, the standard deviation is higher for the catamaran compared to the barge. For all LCs, the barge has the

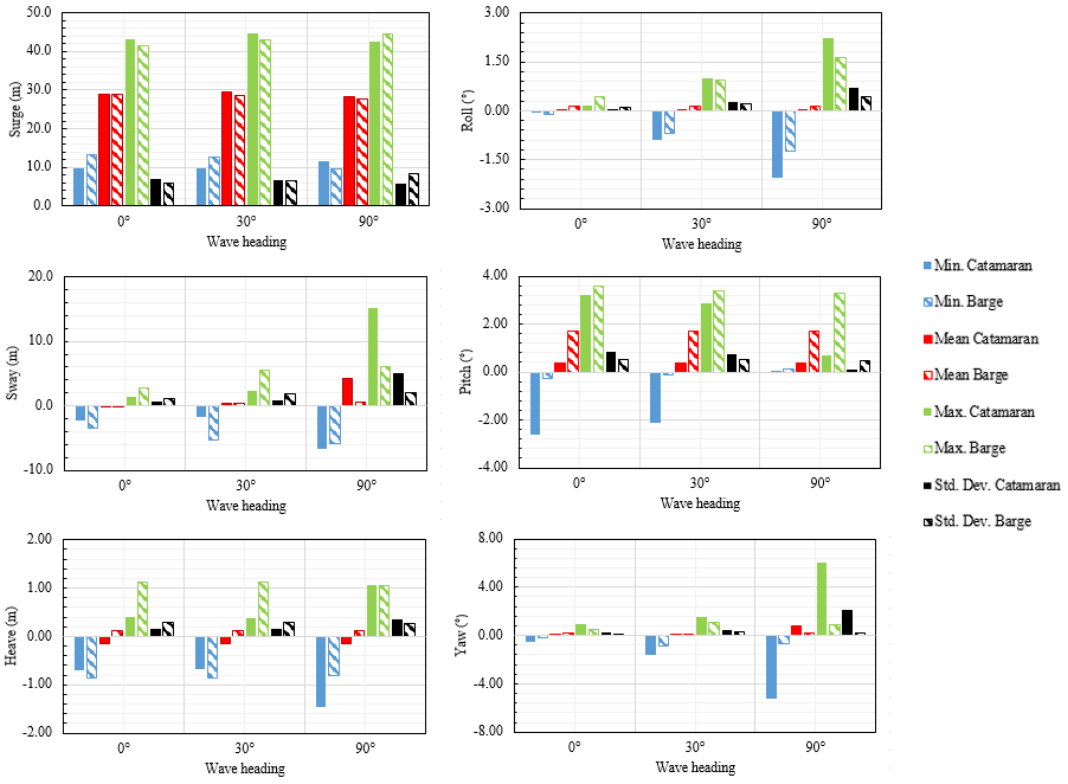

greatest side-side (S-S) tower-base bending moment, which stems from the tangential forces, or aerodynamic drag, that tend to bend the blades and tower in the rotor plane. Comparing the two platforms, the differences in the first two LCs are insignificant. For LC 3 - 5, there is approximately a 15% difference between the S-S tower-base bending moments of the barge and catamaran platforms.

6.6 Incident wave angle at 30° and 90°

This next section presents and discusses the results of LC 6 - 7 which were simulated to investigate the dynamic responses, in terms of platform motions, mooring line tensions, produced power and tower-base bending moments, of the two FOWTs when the alignment between the incoming wind and waves change.

6.6.1 Platform motions

Figures 18 & 19 compare the platform motion time histories of the two platforms under LC 6 – 7, and **Figure 20** charts the platform motion statistics. Considering surge, the mean of both platforms is similar for all wave headings which is approximately a 25-30 m offset. As the wave heading angle goes around the compass, the variation in surge of the catamaran reduces whereas for the barge it increases. For sway mode, this is mirrored with the catamaran fluctuating more compared to the barge. However,

the amplitude of catamaran sway when the waves are incoming at 90° is reasonable with a maximum amplitude of 15 m. The heave response of the barge is similar for all wave headings, meanwhile the variation in heave response of the catamaran noticeably increases when the waves are incoming perpendicular to wind inflow. This is due to entrapped water between the demi-hulls amplifying the heave response as discussed in the previous sections. A maximum heave of 1.5 m is observed which means the effect of this dynamic amplification is insignificant. For roll and pitch motion of the catamaran similar but opposite trends occur. The roll response increases whilst pitch response decreases as the wave heading angle increases towards 90°. The roll behaviour of the barge is similar to the catamaran; however, the pitch behaviour is slightly different in that the response is nearly identical for varying wave headings. This suggests the pitch response of the barge is dominated by wind loading whilst the catamarans pitch response is dependent on wave loading. The yaw response of the catamaran when the wave heading is 90° is much larger compared to the barge. This is because the catamaran is much longer which means it will tend to yaw with incident waves perpendicular to the x-axis. **Figure 20** and **21**, shows the effect of yawing on power generation for the catamaran. When the platform is positioned directly facing the incoming wind, the power produced is 4.9 MW. This is the maximum power the turbine can produce given its efficiency. When the platform is yawed 5°, 10°, and 15°, the produced power is 4.85 MW, 4.71 MW, and 4.50 MW, equating to a reduction of 1%, 3.82%, and 8% in generated power, respectively. Therefore, it can be said that if the platform does not yaw more than 15°, then reduction in power cannot exceed 8%, and for 10°, 3.82% and for 5°, 1%. Under LC 7, the

catamaran only experiences a maximum yaw of 6° during the one-hour simulation for a brief period of time which means that the produced power is not significantly affected.

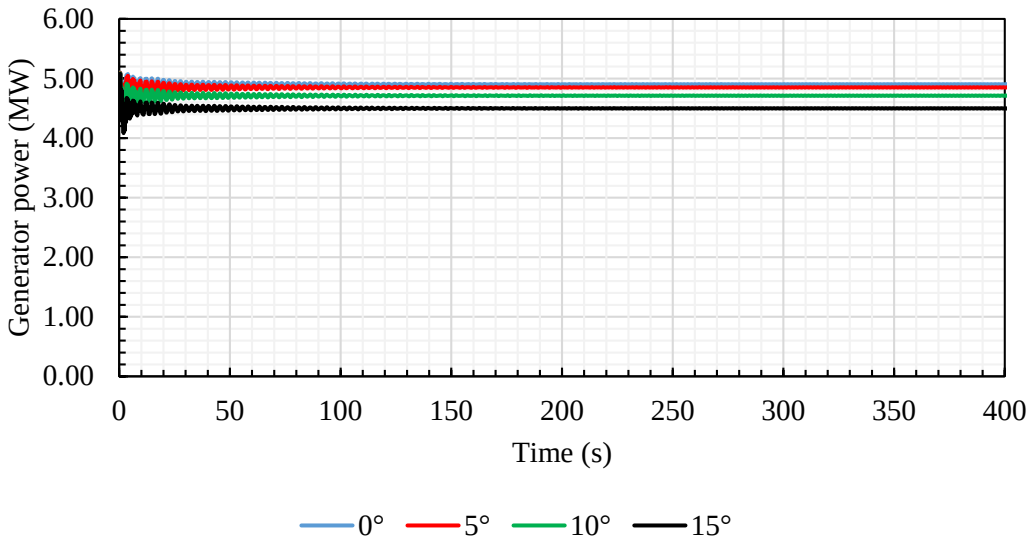

Figure 20. Effect of yawing on power generation.

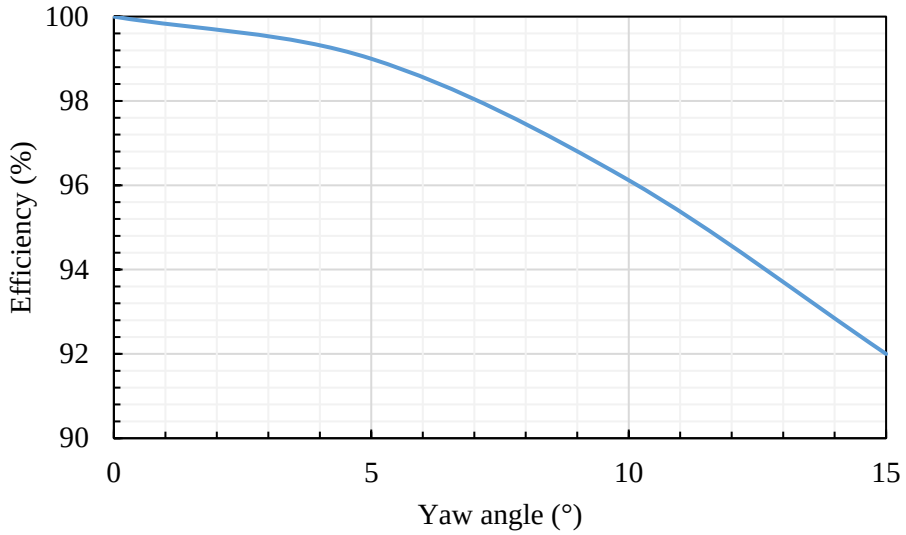

Figure 21. Wind turbine efficiency vs platform yawing.

6.6.2 Mooring tensions

Figure 22 compares the time-domain fairlead tensions of both platforms under LC 6 – 7. Considering LC 6, there is negligible differences in the fairlead tension of all mooring lines between both platforms. The maximum fairlead tension is approximately 0.84 MN. Under LC 7, the waves are

499 incoming perpendicular to the direction of wind flow. The surge response for the catamaran under this
500 load case reduces. As a result, the predicted maximum fairlead tension is lower. Conversely, the surge
501 response of the barge is similar for both load cases and the mooring line tension follows a similar trend
502 in both simulations.

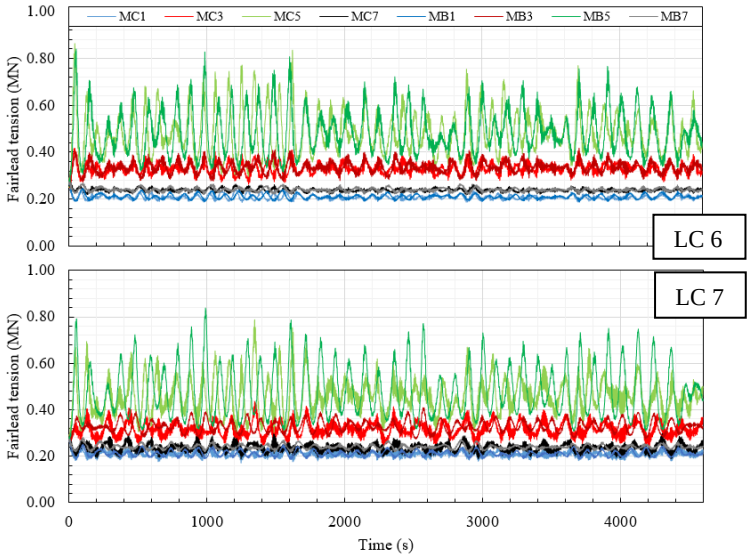

Figure 22. Time-domain fairlead tensions under LC 6 - 7.

503 ### 6.6.3 Power production

504 **Table 7** tabulates the power production statistics under LC 6 – 7, whilst **Figure 23** graphs the
505 generator power time histories of both platforms. From **Table** 7, it can be said that the quality of power
506 produced by the catamaran improves as the misalignment between the incoming wind and waves
507 increases up to 90°. This is because the minimum and mean power produced increases whilst the
508 standard deviation decreases. The maximum produced power also decrease however, this is by a small
509 amount. On the other hand, the quality of power produced by the wind turbine supported by the barge
510 is constant for all wave heading angles. Subject to LC 6 **Figure 21** shows the produced power by the
511 wind turbines supported by operate similarly. Under LC 7, the power generated by the wind turbines
512 follow a similar trend, however the power produced by the wind turbine supported by the catamaran
513 platform is of better-quality power due to less fluctuation.

514 **Table 7.** Power production of both platforms under varying wave headings.

	0°		30°		90°	
	Catamaran	Barge	Catamaran	Barge	Catamaran	Barge
Min.	1.961	1.967	1.955	1.933	2.007	1.917
Mean	4.507389	4.52403	4.520281	4.523217	4.542581	4.518437
Max.	5.184	5.125	5.18	5.111	5.085	5.09
Std. Dev.	0.711707	0.673443	0.694152	0.672026	0.648891	0.674523

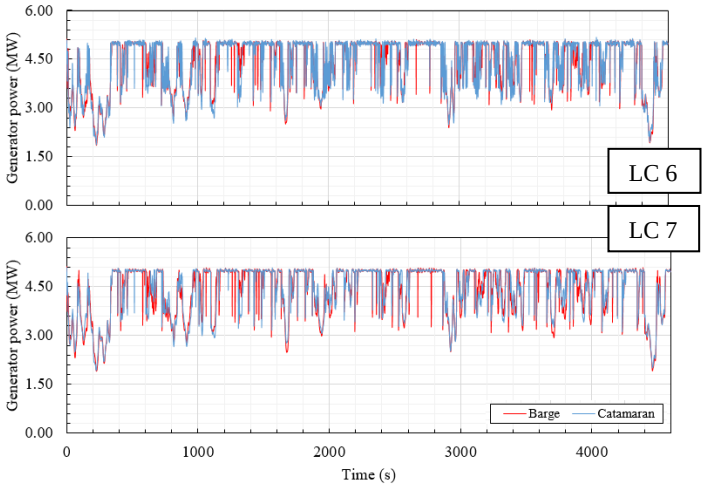

Figure 23. Time-domain generator power of both platforms under LC 6 - 7.

515 ### 6.6.4 Tower-base bending moments

516 **Figure 24** presents the tower-base bending moments about the x- and y-axis of both platforms for
517 30° and 90° wave headings. The results show that the bending moments at the tower-base of the wind
518 turbine supported by the catamaran are smaller and experience less fluctuation compared to the barge
519 for both wave headings. In addition, as the misalignment between the incoming wind and waves
520 increase, the bending moments about the y-axis decreases whilst the bending moment about the x-axis
521 increases for both platforms. This as expected as the wave hydrodynamic loading is the dominant
522 loading.

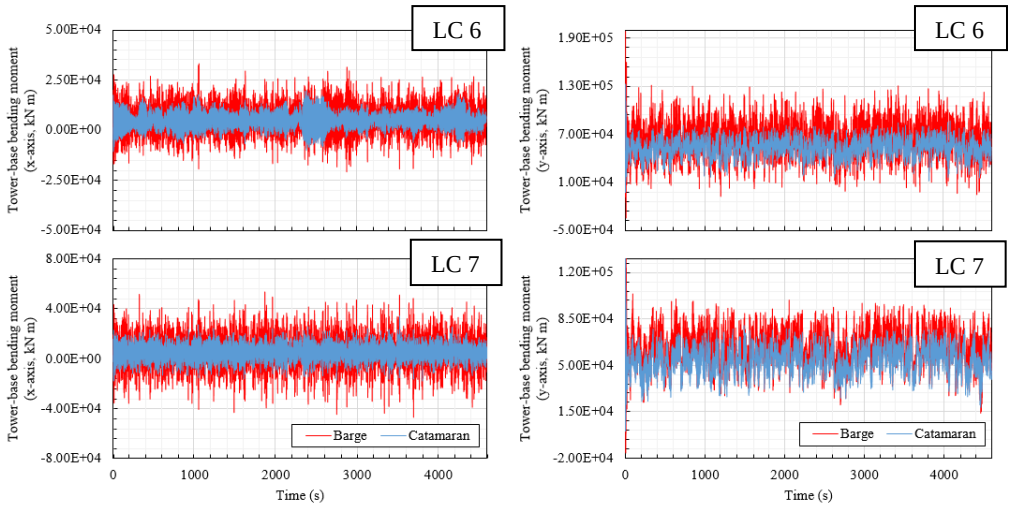

Figure 24. Time-domain tower-base bending moments of both platforms under LC 6 - 7.

7. Conclusions

The hydrodynamic characteristics and dynamic responses of a novel catamaran FOWT operating in intermediate water depth are assessed, and the results are compared with a well-known barge FOWT, the ITI Energy barge. The FOWTs are modelled using OpenFAST and ANSYS AQWA numerical tools coupled via a DLL, namely F2A, to conduct efficient fully coupled aero-hydro-elastic-servo simulations. The current research has revealed advantages which a catamaran-type floater has over a conventional barge-type floater. Firstly, the catamaran has a large deck area; this can be used for other functions such as marine power generation, solar panels, or hydrogen conversion. If utilised properly the additional functionality would ultimately lead to cost reductions. Secondly, evaluation of hydrodynamic characteristics has shown that the catamaran has better hydrodynamic performance over the barge. The catamaran platform has higher sway, roll, pitch, and yaw hydrodynamic coefficients compared to the barge. This mean the catamaran floater has increased hydrodynamic restoring stiffness and damping for these modes of motion. The hydrodynamic coefficients also revealed that a catamaran responds distinctively at certain frequencies for vertical and horizontal plane motions due to symmetric or anti-symmetric interaction, respectively. These frequencies are analogous to the resonant modes of a standing wave between two vertical walls. Moreover, the frequencies are characteristic to the individual platform and depend on demi-hull separation. Findings from the free decay results showed that the catamaran floater increased natural damping in the system for roll and pitch, and especially for pitch damping was increased considerably. This was confirmed in the RAO analysis; the amplitude

observed at the pitch natural frequency of the catamaran floater was reduced by 50% compared to amplitude observed at the pitch natural frequency of the barge. The time-domain simulations showed the response of both platforms were similar for simulated conditions, and that the expected improvement in pitch stability was not necessarily reflected. The reason for this was that the simulated wave periods coincided with the natural pitch period of the catamaran which amplified the platform's dynamic response. Nevertheless, the pitch response of the catamaran was similar to that of the barge. The fact that the catamaran behaves similarly to the barge whilst being excited at its natural frequency highlights the platform's good hydrodynamic performance. One future avenue for research could be how the geometric characteristics of the catamaran floater affect its pitch natural period. The results of this study also showed that the catamaran floater had reduced tower-base bending moments (both F-A and S-S) for all simulated conditions. For rated wind speed (LC 3) and corresponding wave condition, the F-A tower-base bending moment was reduced by 22%. Considering this research was a preliminary investigation into catamaran-type floaters and the design was a first iteration, there is clear evidence that a catamaran floater has advantages over a conventional barge. With optimization and further concept development, it would be anticipated that the performance can be further enhanced which makes this a promising concept to support a wind turbine in intermediate water depths.

Acknowledgements

The authors would like to acknowledge the financial support from the European Regional Development Fund (ERDF), Interreg Atlantic Area (grant number: EAPA_344/2016). Financial support from Liverpool John Moores University is also thanked. The study is also partially supported by the National Nature Science Foundation of China (grant number: 52101317).

References

Aboutalebi, P., M'zoughi, F., Garrido, I., Garrido, A.J., 2021. Performance analysis on the use of oscillating water column in barge-based floating offshore wind turbines. Mathematics 9, 1–22.

Allseas, 2021. Pioneering Spirit.

ANSYS, 2012. AQWA Reference Manual Release 14.5. Canonsburg, USA.

Barooni, M., Ale Ali, N., Ashuri, T., 2018. An open-source comprehensive numerical model for

569 dynamic response and loads analysis of floating offshore wind turbines. Energy 154, 442–454.
570 Brown, S.A., Ransley, E.J., Xie, N., Monk, K., De Angelis, G.M., Nicholls-Lee, R., Guerrini, E.,
571 Greaves, D.M., 2021. On the impact of motion-thrust coupling in floating tidal energy
572 applications. Appl. Energy 282, 116246.
573 Dabssi, N., Chagdali, M., Hémon, A., 2008. Hydrodynamic coefficients and forces on multihulls in
574 shallow water with constant or variable depth. Transport 23, 245–252.
575 Drassanes Dalmau, 2021. 150 Passengers - ECO SLIM.
576 Dzan, W.Y., Chang, S.Y., Hsu, K.C., 2013. Designing and building of a catamaran and its stability
577 analysis. Proc. - 2013 2nd Int. Conf. Robot. Vis. Signal Process. RVSP 2013 148–152.
578 Equinor, 2020. Hywind Scotland.
579 Fang, C.-C., 1996. An Investigation of Motions of Catamarans in Regular Waves.
580 Fang, C.C., Chan, H.S., Incecik, A., 1997. Investigation of motions of catamarans in regular waves -
581 II. Ocean Eng. 24, 949–966.
582 Goupee, A.J., Koo, B.J., Kimball, R.W., Lambrakos, K.F., Dagher, H.J., 2014. Experimental
583 comparison of three floating wind turbine concepts. J. Offshore Mech. Arct. Eng. 136, 1–10.
584 Ideol, 2020a. FLOATGEN.
585 Ideol, 2020b. HIBIKI - Floating wind turbine solution | Japan offshore wind.
586 Johlas, H.M., Martínez-Tossas, L.A., Churchfield, M.J., Lackner, M.A., Schmidt, D.P., 2021. Floating
587 platform effects on power generation in spar and semisubmersible wind turbines. Wind Energy
588 24, 901–916.
589 Jonkman, B.J., Buhl Jr, M.L., 2006. TurbSim User's Guide - Technical Report NREL/TP-500-39797.
590 Jonkman, J., 2007. Dynamics modeling and loads analysis of an offshore floating wind turbine, Ph.D.
591 Thesis.
592 Jonkman, J., Matha, D., 2011. Dynamics of offshore floating wind turbines-analysis of three concepts.
593 Wind Energy 14, 557–569.
594 Jonkman, J.M., 2009. Dynamics of offshore floating wind turbines-model development and
595 verification. Wind Energy 12, 459–492.
596 Jonkman, J.M., Buhl Jr, M.L., 2005. FAST user's guide. Golden, USA.

597 Junianto, S., Mukhtasor, Prastianto, R.W., Wardhana, W., 2020. Motion Responses Analysis for Tidal
598 Current Energy Platform: Quad-Spar and Catamaran Types. China Ocean Eng. 34, 677–687.
599 Lin, Y.H., Yang, C.H., 2020. Hydrodynamic simulation of the semi-submersible wind float by
600 investigating mooring systems in irregular waves. Appl. Sci. 10.
601 Liu, Q. song, Miao, W. pao, Yue, M. nan, Li, C., Wang, B., Ding, Q., 2021. Dynamic Response of
602 Offshore Wind Turbine on 3×3 Barge Array Floating Platform under Extreme Sea Conditions.
603 China Ocean Eng. 35, 186–200.
604 Liu, Y., Li, S., Yi, Q., Chen, D., 2016. Developments in semi-submersible floating foundations
605 supporting wind turbines: A comprehensive review. Renew. Sustain. Energy Rev. 60, 433–449.
606 Loughney, S., Wang, J., Bashir, M., Armin, M., Yang, Y., 2021. Development and application of a
607 multiple-attribute decision-analysis methodology for site selection of floating offshore wind
608 farms on the UK Continental Shelf. Sustain. Energy Technol. Assessments 47.
609 Meng, L., He, Y. ping, Zhao, Y. sheng, Yang, J., Yang, H., Han, Z. long, Yu, L., Mao, W. gang, Du,
610 W. kang, 2020. Dynamic Response of 6MW Spar Type Floating Offshore Wind Turbine by
611 Experiment and Numerical Analyses. China Ocean Eng. 34, 608–620.
612 Murfet, T., Abdussamie, N., 2019. Loads and response of a tension leg platform wind turbine with
613 non-rotating blades: An experimental study. J. Mar. Sci. Eng. 7.
614 National Renewable Energy Laboratory (NREL), 2021. OpenFAST Documentation Release v3.0.0.
615 Olondriz, J., Elorza, I., Jugo, J., Alonso-Quesada, S., Pujana-Arrese, A., 2018. An advanced control
616 technique for floating offshore wind turbines based on more compact barge platforms. Energies
617 11.
618 Principle Power, 2020. WindFloat.
619 Qasim, I., Gao, L., Peng, D., Liu, B., 2018. Catamaran or semi-submersible for floating platform -
620 Selection of a better design. IOP Conf. Ser. Earth Environ. Sci. 121, 0–7.
621 Ramachandran, G.K.V., Robertson, A., Jonkman, J.M., Masciola, M.D., 2013. Investigation of
622 response amplitude operators for floating offshore wind turbines, in: Proceedings of the
623 International Offshore and Polar Engineering Conference. pp. 369–376.
624 Robertson, A., Jonkman, J., Vorpahl, F., Popko, W., Qvist, J., Frøyd, L., Chen, X., Azcona, J.,

625 Uzunoglu, E., Soares, C.G., Luan, C., Yutong, H., Pengcheng, F., Yde, A., Larsen, T., Nichols,
626 J., Builds, R., Lei, L., Nygaard, T.A., Manolas, D., Heege, A., Vatne, S.R., Ormberg, H., Duarte,
627 T., Godreau, C., Hansen, H.F., Nielsen, A.W., Riber, H., Le Cunff, C., Beyer, F., Yamaguchi,
628 A., Jung, K.J., Shin, H., Shi, W., Park, H., Alves, M., Guérinel, M., 2014. Offshore code
629 comparison collaboration continuation within IEA wind task 30: Phase II results regarding a
630 floating semisubmersible wind system, in: Proceedings of the International Conference on
631 Offshore Mechanics and Arctic Engineering - OMAE.
632 Shi, W., Zhang, L., Ning, D., Jiang, Z., Michailides, C., Karimirad, M., 2019. A comparative study on
633 the dynamic response of three semisubmersible floating offshore wind turbines, in: Proceedings
634 of the International Conference on Offshore Mechanics and Arctic Engineering - OMAE.
635 Taboada, J., 2016. Comparative analysis review on Floating Offshore wind Foundations (FOWF).
636 Ing. Nav. 75–87.
637 Thiagarajan, K.P., Dagher, H.J., 2014. A review of floating platform concepts for offshore wind
638 energy generation. J. Offshore Mech. Arct. Eng. 136, 1–6.
639 Wellicome, J.F., Temarel, P., Molland, A.F., Hudson, D.A., 1995. Ship Science Report No.93
640 Theoretical Prediction of the Seakeeping Characteristics of Fast Displacement Catamarans.
641 Yang, Y., 2020. F2A User Manual.
642 Yang, Y., Bashir, M., Li, C., Wang, J., 2021. Investigation on mooring breakage effects of a 5 MW
643 barge-type floating offshore wind turbine using F2A. Ocean Eng. 233.
644 Yang, Y., Bashir, M., Michailides, C., Li, C., Wang, J., 2020. Development and application of an
645 aero-hydro-servo-elastic coupling framework for analysis of floating offshore wind turbines.
646 Renew. Energy 161, 606–625.
647 Zheng, Z., Chen, J., Liang, H., Zhao, Y., Shao, Y., 2020. Hydrodynamic responses of a 6 MW spar-
648 type floating offshore wind turbine in regular waves and uniform current. Fluids 5, 1–28.
649